Interner Bericht
DESY F21-70/2
Juni 1970

Experiments on Deep Inelastic Lepton Proton Scattering

by

F. W. Brasse* and J. May**

* Talk given at the Meeting on Phenomenology and Models of Electromagnetic and Strong Interactions at High Energies, Naples, June 1970.

** Talk given in a modified version at a DESY-Seminar in 1969/70

Interner Bericht
DESY F21/2
Juni 1970

Experiments on Deep Inelastic Lepton Proton Scattering

by

F.W. Brasse*) and J. May**)

*) Talk given at the Meeting on Phenomenology and Models of Electromagnetic and Strong Interactions at High Energies Naples, June 1970.

**) Talk given in a modified version at a DESY-Seminar in 1969/70

Contents:

I. Kinematics

The process e + p → e + p + X is given in the one photon exchange approximation by the following graph:

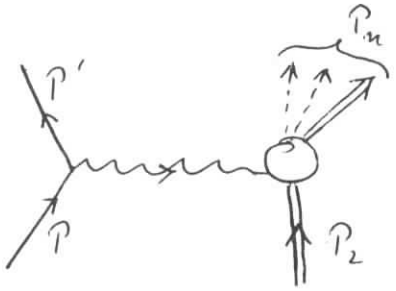

The P, P' and P_i are the four momenta of the involved ingoing and outgoing particles, q is the four momentum of the virtual photon.

For describing the process we need the following variables

$$- q^2 = Q^2 = 4\, EE' \sin^2 \vartheta/2 \,, \qquad (1)$$

the mass of the virtual photon squared,

$$\nu = E - E' = q \cdot P/M \,, \qquad (2)$$

the energy loss of the electron

$$W^2 = 2M\nu + M^2 - Q^2, \qquad (3)$$

the square of the mass of the outgoing pion nucleon system,

and $$\varepsilon = (1 + 2(1 + \nu^2/Q^2)\, tg^2 \vartheta/2)^{-1}, \qquad (4)$$

the polarization of the virtual photon.

ϑ is the scattering angle of the outgoing electron with respect to the incoming one. The polarization depends strongly on this angle. For small angles it is almost always 1.

Furthermore we need

$$K = \nu - Q^2/2M \,, \qquad (5)$$

which is called the aquivalent photon energy, and the scaling variable

$$\omega = \frac{2M\nu}{Q^2} \,. \qquad (6)$$

The cross section for the above process, if one detects only the final electron, can then be written in the form[1)]

$$\frac{d^2\sigma}{d\Omega\, dE'} = \sigma_{Mott} \cdot \left\{ W_2(q^2,\nu) + 2\, W_1(q^2,\nu)\, tg^2\frac{\vartheta}{2} \right\} \quad , \tag{7}$$

where the two form factors or structure functions W_1 and W_2 are functions of the two invariants q^2 and ν and describe the processes at the hadron vertex. σ_{Mott}, the cross section for scattering on a pointlike charge, is

$$\sigma_{Mott} = \frac{\alpha^2}{4E^2} \frac{\cos^2\vartheta/2}{\sin^4\vartheta/2} \quad . \tag{8}$$

Since we are looking for a photoproduction process, it is also possible to write the cross section in terms of the total photoproduction cross sections σ_T for transverse photons and σ_S for longitudinal polarized photons:

$$\frac{d^2\sigma}{d\Omega\, dE'} = \Gamma_T \left(\sigma_T(q^2,\nu) + \varepsilon\, \sigma_S(q^2,\nu) \right) \tag{9}$$

with

$$\Gamma_T = \frac{\alpha}{2\pi^2} \frac{E' K}{E Q^2 (1-\varepsilon)} \quad , \tag{10}$$

the number of virtual photons with transverse polarization per incoming electron. The connections between the form factors and the total cross sections are given by comparing (7) and (9)

$$W_1(q^2,\nu) = \frac{K}{4\pi^2\alpha}\, \sigma_T(q^2,\nu) \tag{11}$$

$$W_2(q^2,\nu) = \frac{K Q^2}{4\pi^2\alpha(Q^2+\nu^2)} \left(\sigma_T(q^2,\nu) + \sigma_S(q^2,\nu) \right) \quad . \tag{12}$$

Introducing the ratio $R = \sigma_S / \sigma_T$ one can write W_2 in the following way

$$W_2 = \frac{1}{\sigma_{Mott}} \cdot \frac{d^2\sigma}{d\Omega\, dE'} \cdot \frac{1}{1 + \frac{2(\nu^2 + Q^2)}{(1+R)\,Q^2} \operatorname{tg}^2 \frac{\vartheta}{2}} \qquad . (13)$$

From this one can get a lower and upper limit for W_2 by $R = 0$ and $R = \infty$:

$$\frac{\varepsilon}{\sigma_{Mott}} \frac{d^2\sigma}{d\Omega\, dE'} \leq W_2 \leq \frac{1}{\sigma_{Mott}} \frac{d^2\sigma}{d\Omega\, dE'} \qquad . (14)$$

This means that W_2 is given by the cross section itself, if ε is close to 1 or $2 \cdot \operatorname{tg}^2 \frac{\vartheta}{2} \ll \left(1 + \frac{\nu^2}{Q^2}\right)^{-1}$.

It is sometimes of interest to look at the cross section for elastic scattering in parallel. This of course contains an extra integration over E':

$$\frac{d\sigma}{d\Omega} = \sigma_{Mott} \cdot \frac{E'}{E} \left\{ \frac{G_E^2 + \tau G_M^2}{1+\tau} + 2\tau G_M^2 \operatorname{tg}^2 \frac{\vartheta}{2} \right\} \qquad (15)$$

with $\tau = \frac{Q^2}{4M^2}$ or, using the polarization parameter ε ,

$$\frac{d\sigma}{d\Omega} = \frac{2\alpha^2 E'^2}{E^2 Q^2 (1-\varepsilon)} \left\{ \tau G_M^2 + \varepsilon G_E^2 \right\} \qquad . (16)$$

W_1 or σ_T corresponds to G_M^2 and σ_ℓ corresponds to G_E^2.

In order to separate the inelastic form factors one has to make measurements for the same value of ν and q^2 at at least two different angles as it is known from elastic scattering.

For μ-p scattering, which should give the same information as e-p scattering, all formulas are basically the same. Only where the electron mass was neglected, the mass of the muon should stay (in Γ_t, σ_{Mott} and φ).
The definition of deep inelastic is not so very clear. But it is common to say that it starts above the main resonance region, which means at $W \gtrapprox 2$ GeV, and at not too small momentum transfers (perhaps $q^2 \gtrsim 1(\mathrm{GeV/c})^2$).

II. Experimental methods and problems

We will come now to the experiments, which have been done so far mainly at SLAC[2], some also at DESY.[3] First we will describe briefly how the experiments were made and what the main difficulties have been.

It is clear that one has to define momentum and angles of the secondary electron. Together with the known primary energy the virtual photon and by this also the mass W of the outgoing hadronic system is then defined. For electron scattering focussing magnetic spectrometers have been used, where angles and momenta are determined by counter hodoscopes and the electrons are defined by Cerenkov- and/or shower counters. These spectrometers can handle large particle fluxes. The μ-proton scattering measurements at SLAC[4] were done by using large spark chambers together with a large aperture magnet. This was necessary because the flux of primary muons was much smaller than that of electrons (about 10^5 muons/sec compared with about 10^{13} electrons/sec).

Some of the main difficulties for these experiments were for example:

1) At DESY[3] the measurements were done with the internal beam of the synchrotron to make use of the fact that the electrons can pass several times through the same target, so having effectively a longer target. But in this case it is difficult to measure the number of electrons in the beam with sufficiently accuracy. Therefore this was indirectly done by referring to elastic scattering measurements at sufficiently low momentum transfer where the form factors are known very well. These measurements were done alternatively with the inelastic measurements. A quantameter, measuring the Bremsstrahlung from the target, was used as a relative monitor.

2) At SLAC[2] there was also a problem with monitoring, because the high intensity beam heated up the target; so the precise density of the target was also indirectly measured by elastic scattering, which was done simultaneously with a second spectrometer.

3) At both places for lower values of secondary energies the flux of electrons through the spectrometers, coming from π^0-decay and pair production, became an appreciable amount of the inelastic scattering rate. A subtraction was made by making measurements with reversed polarity of the spectrometer and setting the positron rate equal to the electron rate, which should be subtracted.

4) In the case of muon scattering the difficulty is to distinguish the scattered muons from hadrons. This was done by using a set of spark chambers with iron plates before and in between to stop the hadrons. They were stopped with an efficiency of 97%.

Since one is interested in measuring the form factors as function of q^2 and ν, one should have a look at the q^2,ν-plane to find out at which values to measure (Fig. 1). In this plane curves of constant W, primary energy and angle ϑ are straight lines. Also keeping the scaling variable ω constant gives a straight line. Normally a total spectrum is taken by keeping E and ϑ fixed and changing the spectrometer momentum from a highest value to the lowest possible one. This means the spectrum starts at elastic scattering, goes across the resonances and ends at some large value of W. While W increases the momentum transfer decreases. Such measurements have been made for 6°, 10°, 18°, 26° and 34° at SLAC[2] for various primary energies as we can see in the next slide (Fig.2). The measurements cover almost completely the area shown. At DESY[3] measurements of this type with fixed E were made only at larger angles (48° and 76°) and of course only up to 6 GeV, which means mainly in the resonance region. But also some spectra were taken at similar angles with fixed momentum transfers of $q^2 \approx 0.8$ and 1.9 $(\mathrm{GeV/c})^2$. For this the energy of the synchrotron had to be changed in small steps.

If one does this for different angles one is able to separate W_1 and W_2 along the whole spectrum, while for the other type

of spectra one has to look for as many crossing points in the q^2, ν-plane as possible in order to lay out the experiment. Fig. 3 shows a spectrum with fixed momentum transfer, measured at DESY. The first resonance is still prominent, also the next ones can be seen. The large errors at the end of the spectrum are due to subtraction of large positron rates and empty target rates.

Before coming to another source of difficulty and errors, the radiative corrections, we would like to show also spectra, taken at SLAC, where the primary energy is fixed (Fig. 4). The momentum transfer changes along the spectra. Comparing the three different spectra one gets already a first impression about the behaviour of the cross sections. At small momentum transfer the resonances with their background are very dominant. At high momentum transfer however the high W range is dominant.

This is not the place to go into details about radiative corrections. However, while for elastic scattering this correction is no problem at all, for inelastic scattering it can be a major difficulty. The reason is the following:
The emission of photons during the scattering process is given by the two diagrams  . The photons are mainly emitted in the directions of the primary and secondary electron (peaking approximation). In the first case the primary energy at the vertex is lowered, in the second case the secondary energy at the vertex was higher than the measured one.

Looking at the E, E'-plane

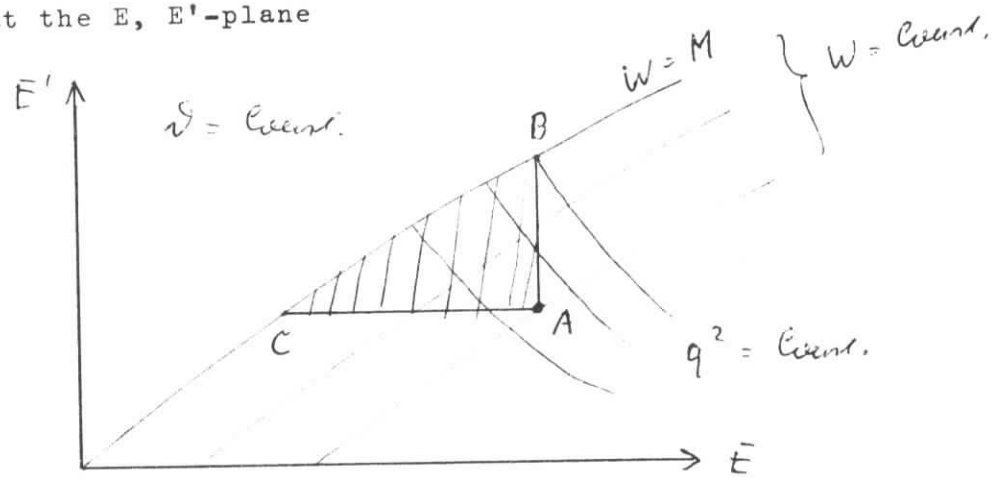

one has again curves for constant W and constant q^2. If one measures a spectrum for constant ϑ and E one gets contribution by radiative tails from the whole shaded area ABC, especially also from the elastic curve. In addition one has a correction due to the radiative tails, which originate along the line A B. In order to do corrections properly one has to know the dependance of the cross section on W and q^2 in the whole area A B C. This means that one has to move somewhat continuously into a new area. Since momentum transfer is decreasing along A C one gets the largest corrections from there. It is a luck that the inelastic cross sections in the deep inelastic region are so big. Fortunately also one does not have to know cross sections at other scattering angles (in the peaking approximation).

Fig.5 shows a comparision of spectra without and with radiative corrections and the total corrections itself, which goes up to 40% at the end of the spectrum.

For the contribution from the elastic tail one is able to calculate the corrections without approximations, whereas in the inelastic region one uses the peaking approximation.

III. Discussion of experimental data

Before we come to the discussion of the data in the deep inelastic region it may be good to bring back to our memory some features of the resonance region[5] (Fig. 6). Here the photoabsorption cross sections for the dominant resonances are plotted against q^2. The connecting lines are lines of constant momentum transfer. Whereas at small momentum transfer the cross section decreases with W, at high momentum transfer it increases. The values shown are the resonances including the background underneath. By comparing the bumps in the spectra one can roughly say that the two parts itself show the same behaviour.

a) The q^2 and ν dependance of the SLAC data.

We will now discuss the SLAC data. So far only the 6° and 10° data are published numerically. 18° data do only exist in a preliminary form[6]. The higher anlges 26° and 34° have been used by the SLAC group for some preliminary σ_S, σ_T separations, given at the Daresbury conference[7] in the form $R = \sigma_S/\sigma_T$ only.

In the next Fig. 7 cross sections normalized by σ_{Mott} for different values of W above the resonance region are compared with eachother and with elastic scattering in their dependance on q^2. The dramatic change of the elastic scattering is slowed down to almost constant structure functions at W = 3,5 GeV.

Making assumptions about R it is possible to calculate W_2 from $\frac{\mathrm{d}^2\sigma}{\mathrm{d}\Omega\,\mathrm{d}E'}$. For the small angle data W_2 should then not depend too much on R. In the following Fig. 8 the dimensionless quantity νW_2 is plotted against ν for various values

of q^2 for the 6° and 10° data with R = 0 and R = 0.5. The zero of the scale for νW_2 is suppressed. The values of W, the mass of the total hadronic system, are also marked down. In all four cases the data are covering about the same range of W. At small momentum transfer the function νW_2 is falling down with increasing ν whereas at high momentum transfer it is going up. For R = 0 it does not go above 0.34. For R = 0.5 all values are higher, the difference is increasing with increasing ν. The drastic change of the data while going from $q^2 = 2$ to $q^2 = 4$ $(GeV/c)^2$ looks very peculiar, but as we will see later, this is a general feature of the behaviour of the structure functions. We may also keep in mind that for $q^2 = 2.0$ $(GeV/c)^2$, where we have mainly only 10° data, νW_2 seems to be constant as a function of ν.

b) The scaling of νW_2

Bjorken[8] has shown by relating the structure functions to matrix elements of commutators of currents at almost-equal times at infinite momentum that the structure functions should depend for large values of q^2 and ν, but finite values of ν/q^2, only on this ratio $\frac{\nu}{q^2}$:

$$\nu W_2(q^2,\nu) \xrightarrow[q^2,\nu\to\infty]{} F_2\left(\frac{\nu}{q^2}\right) \qquad (17)$$

$$W_1(q^2,\nu) \xrightarrow[q^2,\nu\to\infty]{} F_1\left(\frac{\nu}{q^2}\right)$$

The limit $q^2 \to \infty$ and $\nu \to \infty$ is generally called the Bjorken limit.

The next Fig. 9 shows νW_2 for the 6° data from SLAC as function of $\omega = \frac{2M\nu}{q^2}$ in a) only for E = 7 GeV (which means $q^2 < 0.5$ $(GeV/c)^2$), in b) for higher energies with the assumption R = ∞ and in c) with R = 0. If indeed R is close to zero, then data for different q^2 or ν, but same ω are very close. But one should note that points with smaller primary energy, which means smaller q^2 at the same ω, above $\omega = 4$ are generally lying lower than those with higher primary energy. The 10° data are shown in Fig. 10. The evaluation of νW_2 is more sensitive here to R. But again one can say, if R is small, then the data are consistent with scaling. The momentum transfers are in general higher here at the same values of ω than for the 6° data. To see a remaining q^2-dependance is difficult because of the errors. Whereas the 6° fall down above $\omega = 5$, these stay constant. But this difference may be due to a momentum transfer still too small in case of the 6° data. The conclusion could be, if R is small, that νW_2 is scaling and in addition getting constant in ω and therefore also in ν and q^2, if q^2 and ν are large enough. But of course for much higher values of ω (for large q^2 also) νW_2 could still change.

Even in the resonance region there seems to be some kind of scaling at least for the background. With increasing primary energy the resonances are more and more moving down the curve towards $\omega = 1$. We will come back to this region later again.

c) What is known about $R = \sigma_S / \sigma_T$?

In order to separate σ_S from σ_T, small angle data have to be compared with large angle data. This has been done in the next Fig. 11 for SLAC and DESY data.[9] $\sigma_T + \varepsilon \sigma_S$ is plotted versus ε, which should give a straight line. The slope is equal to σ_S, which is quite small in all cases with respect to σ_T.
In Fig. 12 we see the SLAC small angle data compared with their larger ones, which are preliminary[7].R does not exceed 0.5. In the pictures there are also shown predictions by the VDM, calculated by Sakurai[10]. This is the only model among the many others, which gives definite predictions for the cross section. According to the following diagram

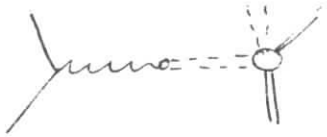

the virual photon is coupled to a vector meson, which then interacts with the proton. Assuming that the hadronic matrix element varies very little with q^2 Sakurai gets for σ_T only the ρ -propagator as q^2 dependence and for σ_S an additional factor q^2, which makes it zero in the limit of real photoproduction. So he gets the relation

$$R = \xi(K) \frac{q^2}{m_\rho^2} \left[1 - \frac{1}{\omega}\right]^2 \qquad (18)$$

with $\xi(K) = \sigma_{\rho p}^{\parallel}(K) / \sigma_{\rho p}^{\perp}(K)$, the ratio of total cross sections on protons for longitudinal and transversely polarized ρ mesons, which are expected to vary very little with K.

The extra factor in brackets in (18) comes in due to a special choice of frame, which is for example not obtained by Fraas and Schildknecht,[11] using helicity amplitudes.

Coming back to the data, we see that R comes out much too big in the VDM and σ_T, which falls in this model roughly with $1/q^4$, much too small.

In the next figure Fig. 13 we see a summary of the preliminary status on the determination of R. It is very unlikely that R can be in this range of ω and q^2 larger than 0.5. The average value is about 0.2. In their last paper Cho and Sakurai[12] claim that the success of VDM for inelastic electro production should be better, if $W^2 \gg q^2$ or $\omega \gtrsim 10$. So this range would just start at the end of the range we have in Fig. 13. The prediction would be 2,5, using $\xi = 1.22$ as determined from the slope of the inelastic data at very low values of q^2. This value has to be compared with an experimental one of about 0.2.

d) Final conclusions from the data

In Fig. 14 all 6° and 10° values of νW_2 for $W \geq 2$ GeV and $q^2 \geq 1$ (GeV/c)^2, calculated with R = 0,2, are plotted against ω. Within the error bars and the available range of q^2 at the different places in ω scaling is fulfilled. Above $\omega = 5$ νW_2 seems to fall down a little. For R = 0 the SLAC group[13] has made a fit to the values for $\omega > 5$, and get a statistically significant decrease of W_2 (2,5 stand. dev.). But for R = 0.2 this should be less.

The almost constant part of νW_2 leads to the following behaviour of σ_T, neglecting the small contribution of σ_S to W_2,

$$\left.\begin{array}{l} \sigma_T \propto \frac{1}{Q^2} \\ \sigma_T \to \text{constant in } \nu \end{array}\right\} \text{for } \begin{array}{l} \omega > 5, \\ Q^2 \geq 1\,(\text{GeV/c})^2. \end{array} \qquad (19)$$

e) Comparison with resonance region

We would like to come back once more to the resonance region. In Fig. 15 and 16 νW_2 is plotted again against ω using the small angle data of SLAC only for W > 2 GeV and some large angle data from DESY[3)5)14)]. For both νW_2 is calculated with R = 0.2. It is surprising how well these values, except for the resonance peaks itself, also lie on top of each other. If one uses larger values of R, this is not as good, since the large angle data are sensitive to this. The background in the resonance region seems to scale in itself and with the region above the resonances, if in both regions longitudinal contributions are small.

It is also possible to calculate W_1 with the assumption R = 0.2. $\frac{q^2}{\nu} W_1$, which is shown in Fig. 17, is with R = 0,2 almost identical with νW_2, especially the shape is the same. The resonance region does not fit as well to the region above the resonances as it is true for νW_2. But the small angle data are now more sensitive to R, since $\frac{d^2\sigma}{d\Omega\, dE'}$ does not depend very much on W_1 for small angles. If however scaling for the nonresonant

parts is true for both structure functions, then exact equality of νW_2 and $\frac{q^2}{\nu} W_1$ is excluded and could only be reached in the limits $q^2 \to 0$ and $q^2 \to \infty$.

IV. Inelastic μ-proton scattering

Inelastic μ-proton scattering has been done at SLAC by Dieterle et al.[4]. A summary of their measurements is given in Fig. 18, where the photoabsorption cross section $\frac{1}{\Gamma_T} \cdot \frac{d^2\sigma}{d\Omega dE'} = \sigma_{exp}(q^2, K)$ is plotted against q^2. Also shown are the cross sections for real photons, averaged over the results of different laboratories. The curves are fits, made by the authors, of the form

$$\sigma_{exp} = \sigma_i(K) \cdot \frac{1}{1 + \frac{q^2}{\mu^2}} \qquad (20)$$

with the mass μ kept independent from K and resulting in $\mu = 0{,}85$ GeV. There is however no reason for taking the same value of μ in the resonance region as above. For large values of K and q^2 the q^2-dependence is qualitatively the same as in electron proton scattering. A separation of σ_S and σ_T was not possible, because measurements were only made at small scattering angles.

V. Futher comparison with some theoretical models

We would like to talk now briefly about a few main theoretical models, to be able to compare them with the data and to see, what one can learn from them for new experiments in this field, which are planned at various laboratories.

There is at first the parton model, which was first developped by Feynman, and then worked out by Bjorken and Paschos[15]. The basic idea is to see the scattering in a frame, in which the proton has infinite momentum. The electron-proton center-of-mass frame is at high energies of the electron a good approximation to such a frame. The proton is thought to be built up by pointlike constituents or "partons", whose relative motion is slowed down by the time-dilatation in this frame. The virtual photon interacts then with one of these structureless, free partons, which carries a fraction x·P of the total momentum P, according to the following diagram:

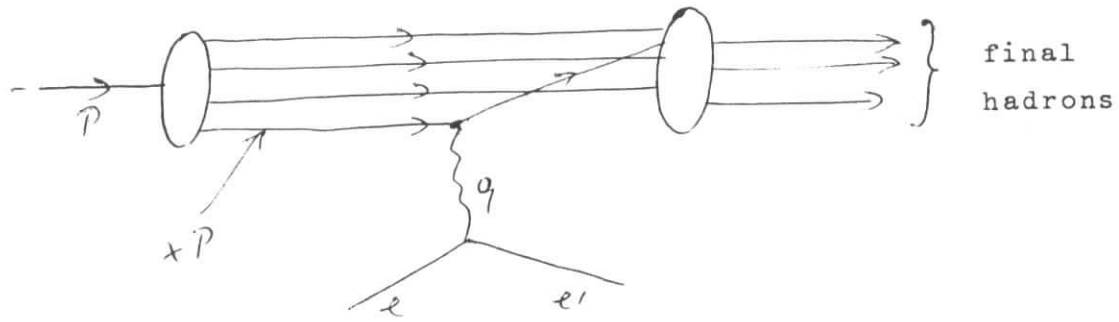

Then in a final state interaction the outgoing physical hadrons are produced. Ff $Q^2 >> M^2$, the scattering from individual partons should be incoherent. The contribution from an individual parton to W_2 is $W_2^{(i)} = Q_i^2 \delta\left(\nu - \frac{Q^2}{2Mx_i}\right)$, which is scattering on a pointlike particle depending only on one variable.

The results, obtained by Bjorken and Paschos, are

$$\nu W_2(\nu, q^2) = \sum_N P(N) \left\langle \sum_i q_i^2 \right\rangle_N \times f_N(x) \equiv F(x) \qquad (21)$$

with $x = \frac{Q^2}{2M\nu} = \frac{1}{\omega}$,

$P(N)$ = probability to find N partons in the proton,

$\left\langle \sum_i q_i^2 \right\rangle_N$ = average value of sume of the charges of these N partons,

and $f_N(x)$ = probability of finding among these N partons a parton with longitudinal fraction x of the proton's momentum.

Equation (21) means scaling for νW_2.

Furthermore they get

$$\begin{aligned} \sigma_S &= 0 \quad \text{for spin } 1/2 \text{ partons}, \\ \sigma_T &= 0 \quad \text{for spin } 0 \text{ partons}. \end{aligned} \qquad (22)$$

The last condition is easy to understand, if one remembers that σ_T corresponds to magnetic scattering. For the first one can argue that in the infinite momentum frame one has in this case only backward magnetic scattering leading in the laboratory frame to zero for the scalar part.

Integration of (21) gives the sume rule

$$\int dx\, F(x) = \sum_N P(N) \frac{\left\langle \sum_i q_i^2 \right\rangle_N}{N} \qquad (23)$$

= mean-square charge per parton.

Specific results for this and the ratio of σ_n / σ_p are obtained by making assumptions for the partons, as for example the proton built up by three quarks with a distribution of quark-antiquark pairs. In Table I the predictions are summarized and compared with experiment.

Another interesting model is the fieldtheoretical model by Drell, Levy and Yan.[16] They also use the infinite momentum frame and the parton picture of the proton, where the constituents are seen pointlike by the virtual photon, if ν and q^2 are large enough (in the Bjorken limit). The above parton diagram is modified to

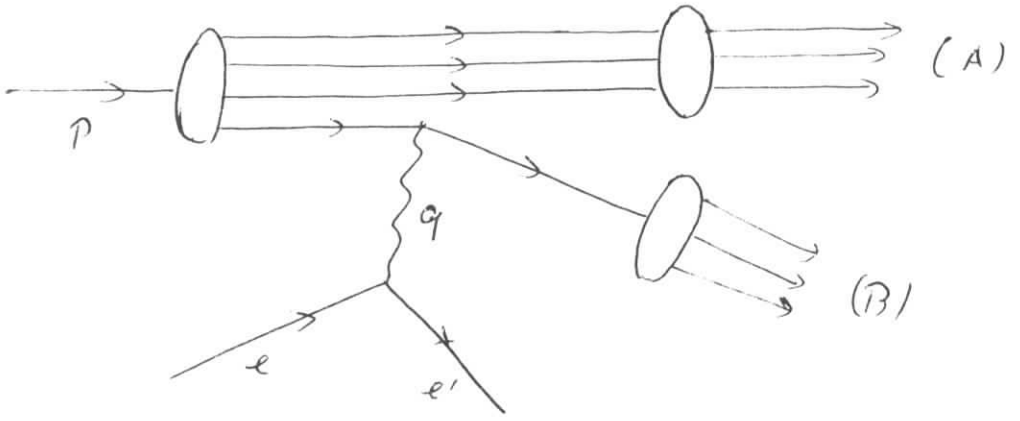

Two groups of particles are built up, which do not interact with each other because they are separated by a large momentum transfer q^2. In the laboratory frame there will be these two groups of particles, where group (B) is travelling along the direction of the virtual photon $\vec{q}$ with high momentum, leaving the group (A) behind it. Using perturbation theory with g_s coupling and assuming a cutoff for all transverse momenta they derive scaling for νW_2 and W_1 in the Bjorken limit. For $\omega \to \infty$ in addition they derive, that the proton is built up by bare protons itself, to which the photon is coupled. An interesting conclusion then is that $\sigma_S = 0$ for $\omega \to \infty$ (partons have spin 1/2). A summary of conclusions from this model is also given in Table I.

For the diffraction model Harari [17] has given a list of predictions, where some of them are a combined result of parton and diffraction model. Harari suggests that the s-channel resonances or the exchange of ordinary trajectories (P', A_2,...) in the t-channel, which correspond to each other, should vanish with a high power of q^2 (like Formfactors), so that the exchange of the Pomeranshukon or the nonresonating background in the s-channel is left over as the only important contribution. At large momentum transfers the scattering should be purely diffractive and the photoabsorption cross section should become constant as function of ν for $\nu \to \infty$ and q^2 large, but fixed:

$$\sigma_T, \sigma_S \to \text{constant in } \nu \quad \text{for } \nu \text{ and } q^2 \text{ large.}$$

Assuming scaling for νW_2 and W_1 this means

$$\sigma_T \propto \frac{1}{q^2} \qquad (24)$$

We remember that the experimental data are not in contradiction to this. There is no prediction for the ratio R. Specific diffractive channels like ρ-production should also behave like (24), whereas specific nondiffractive channels like single π-production should vanish with a higher power of q^2. The main predictions are again summarized in Table I.

The VDM as a special case of the diffraction model was already discussed in part IIIc.

VI. Further experiments in the deep inelastic region

There are three types of experiments, which are being planned or which have started already and which might clearify the situation in the deep inelastic region. This is at first the electron neutron scattering without detecting the final hadronic system. It is being done at SLAC by the same group, which did the electron proton scattering. To see the difference of $\sigma_n / \sigma_p = 0.8$ might however be difficult, since it has to be done on deuterium.

The second type are experiments, where one hadron will be detected in coincidence with the scattered electron with the definition of its parameters so that the rest mass can be determined. These experiments are planned at NINA[18] and at DESY,[19] but due to the low energy more or less only at the beginning of the deep inelastic region. One would get information about the contributions from specific channels like ρ's or from partons in Drells specific picture, where fast protons in the direction of the virtual photon dominate the total cross section.

In the third class of experiments, where large aperture spark chambers are used, more than one of the final hadrons can be detected. One of this type is running at DESY,[20] but at first with perhaps a too low momentum transfer, and a second one is planned at SLAC.[21] These should give all the information needed to understand the complete behaviour.

References

1) R. von Gehlen, Phys. Rev. 118, 1455(1960);
M. Gourdin, Nuovo Cim. 21, 1094 (1961)

2) E.D. Bloom, D.H. Coward, H. DeStaebler, J.Drees, G.Miller, L.W. Mo, R.E. Taylor, M. Breidenbach, J.I. Friedman, G.C. Hartmann, H.W. Kendall, Phys. Rev. Lett. 23, 930, 1969, SLAC-PUB-642 August 1969

3) W. Albrecht, F.W. Brasse, H. Dorner, W. Flauger, K.H. Frank, E. Ganssauge, J. Gayler, H. Hultschig, and J. May, Nuclear Physics B13 (1969) 1-8, DESY 69/7

4) B.D. Dieterle, T. Braunstein, J. Cox, F. Martin, W.T. Toner, M.L. Perl, T.F. Zipf, W.L. Lakin, H.C. Bryant, SLAC-PUB-651 August 1969

5) W. Albrecht, F.W. Brasse, H. Dorner, W. Flauger, K. Frank, E. Ganssauge, J. Gayler, H. Hultschig, and J. May, Physics Letter 3 (1968) 225-228, DESY 68/48

6) J. Drees, private communication

7) R.E. Taylor, Proceedings of the 4th International Symposium on Electron and Photon Interactions at High Energies, Liverpool, 1969

8) J.D. Bjorken, Phys. Rev. 179 S. 1547 (1969), SLAC-PUB-510 September 1968

9) W. Albrecht, F.W. Brasse, H. Dorner, W. Flauger, K.H. Frank, E. Ganssauge, J. Gayler, H. Hultschig, V. Korbel, and J. May, DESY 69/46

10) J.J. Sakurai, Phys. Rev. Lett. 22, 981, 1969

11) H. Fraas, D. Schildknecht, DESY 69/18

References (2)

12) C.F. Cho and J.J. Sakurai, Preprint 1969

13) M. Breidenbach, J.I. Friedman, H.W. Kendall, E.D. Bloom, D.H. Coward, H. DeStaebler, J. Drees, L.W. Mo, R.E. Taylor, Phys. Rev. Lett. 23, 935, 1969

14) F.W. Brasse, J. Engler, E. Ganssauge, and M.Schweitzer, Nuovo Cimento 55A (1968) 679-689, DESY 67/34

15) J.D. Bjorken and E.A. Paschos, SLAC-PUB-572 April 1969

16) Sidney D. Drell, Donald J. Levy, and Tung-Mow Yan, Phys. Rev. Lett. 22, 744, 1969
and
Sidney D. Drell, Donald J. Levy, Tung-Mow Yan, SLAC PUB 645 September 1969

17) Haim Harari, Phys. Rev. Lett. 22, 1078, 1969
and
Haim Harari, Phys. Rev. Lett. 24, 286, 1970

18) NINA-Proposal DNPL/SCP 55

19) DESY-Proposal Nr. 91

20) DESY-Proposal Nr. 85

21) SLAC-Proposal Nr. 65

TABLE I

MODEL / FEATURE	PARTONS Bjorken, Paschos	FIELD THEO. MOD. Drell, Levy Yan	DIFFR. Harari	EXPER.
Scaling	Yes	Yes	--	Yes
$\int \nu W_2 dx$	$\gtrsim .22$ (3 quark in sea of $q\bar{q}$)	--	.22	$.17 \pm 0.1$
$\int \frac{\nu W_2}{x} dx$	∞	>1	∞	$>.72 \pm 0.1$
σ_ℓ / σ_t	$S=0 \to \infty$ $S=1/2 \to 0$	0	?	~ 0.2
Particles along $\vec{q}$	Depends on σ_ℓ / σ_t	Mostly Protons for $\omega \to \infty$	π from ρ, ω for $q^2 \to \infty$	?
σ_n / σ_p	0.8 (Quark) and 1 as $\frac{\nu}{Q^2} \to \infty$	1 for $\omega \to \infty$	1	?
ν-dependance	?	?	σ_T constant for q^2 large	constant for $5 < \omega < 20$
q^2-dependance	?	?	$\sigma_T \propto \frac{1}{q^2}$ if scaling	$\frac{1}{q^2}$

Figure captions

Fig. 1: Kinematics in the q^2, ν-plane

Fig. 2: Kinematics of the SLAC measurements in the q^2, ν-plane

Fig. 3: Inelastic spectrum taken at fixed four momentum transfer of $q^2 = 0.773\ (GeV/c)^2$

Fig. 4: Inelastic spectra taken at fixed primary energies

Fig. 5: Spectrum a) without and b) with radiative corrections. Curve c) gives the total radiative correction. The dotted line in a) is the contribution from elastic scattering.

Fig. 6: Photoabsorption cross section for the main resonances as function of the four momentum transfer q^2.

Fig. 7: The cross section, normalized to the Mott cross section, for various masses W compared with elastic scattering.

Fig. 8: νW_2 as function of ν for the SLAC measurements for various ranges of q^2.

Fig. 9: νW_2 as function of $\omega = 2M\nu/q^2$ for the 6° data.

Fig. 10: νW_2 as function of $\omega = 2M\nu/q^2$ for the 10° data.

Fig. 11: $\sigma_T + \varepsilon\sigma_S$ as function of ε for SLAC and DESY measurements.

Fig. 12: $\sigma_T + \varepsilon\sigma_S$ as function of ε for SLAC measurements.

Fig. 13: $R = \sigma_S/\sigma_T$ as function of ω.

Fig. 14: νW_2 as function of ω for 6° and 10° data with $R = 0.2$

Fig. 15 and 16: Comparison of νW_2 in the high energy small angle range with resonance large angle range. Assumption for all $R = 0.2$

Figure captions (2)

Fig. 17: Comparison of $\frac{q^2}{\nu} W_1$ in the high energy small angle range with resonance large angle range. Assumption for all R = 0.2

Fig. 18: Results from μ-p scattering

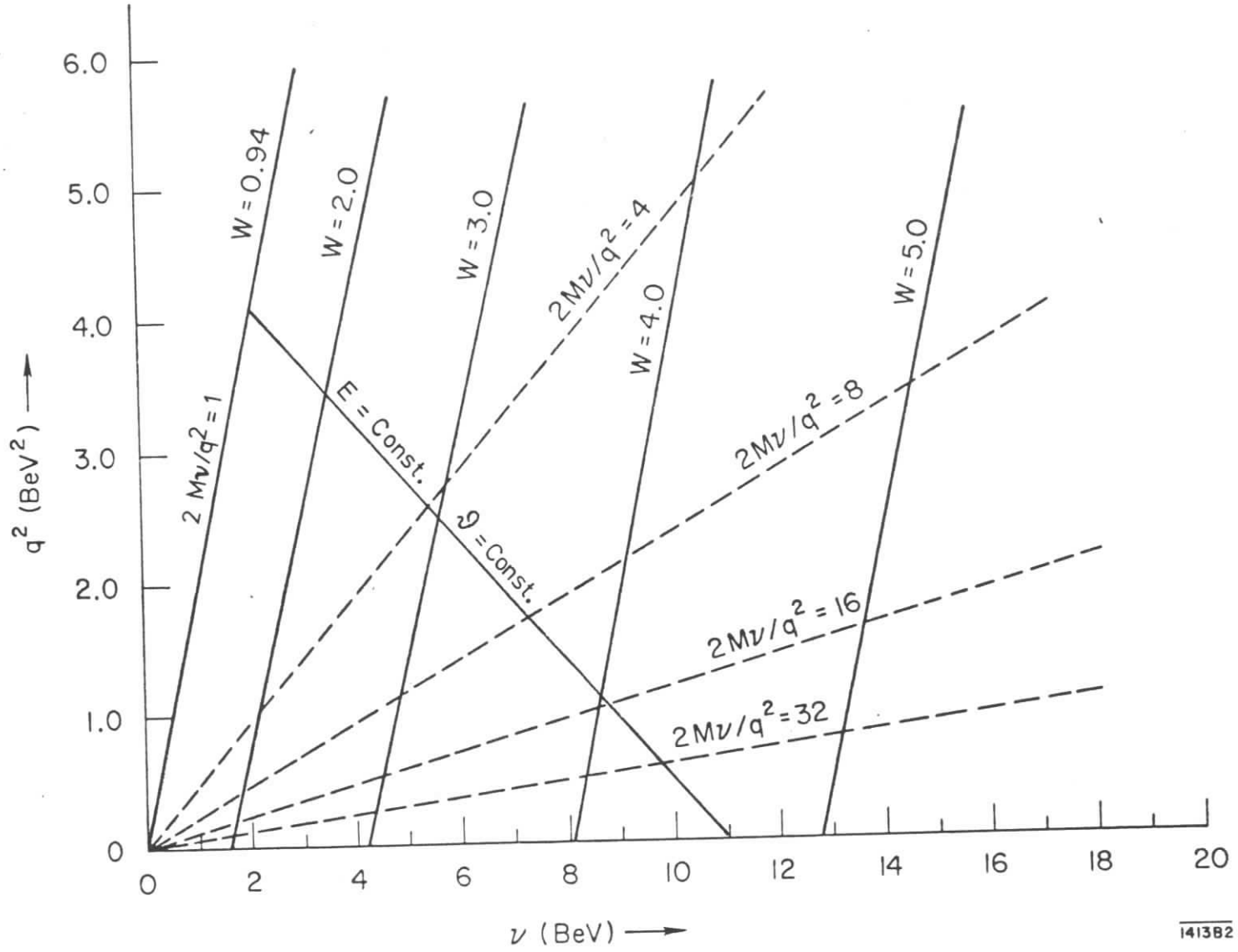
6.0
5.0
4.0
3.0
2.0
1.0
0
q^2 (BeV^2) ⟶
0
2
4
6
8
10
12
14
16
18
20
ν (BeV) ⟶
W = 0.94
W = 2.0
W = 3.0
W = 4.0
W = 5.0
2 Mν/q² = 1
2Mν/q² = 4
2Mν/q² = 8
2Mν/q² = 16
2Mν/q² = 32
E = Const.
ϑ = Const.
141382

Fig. 1

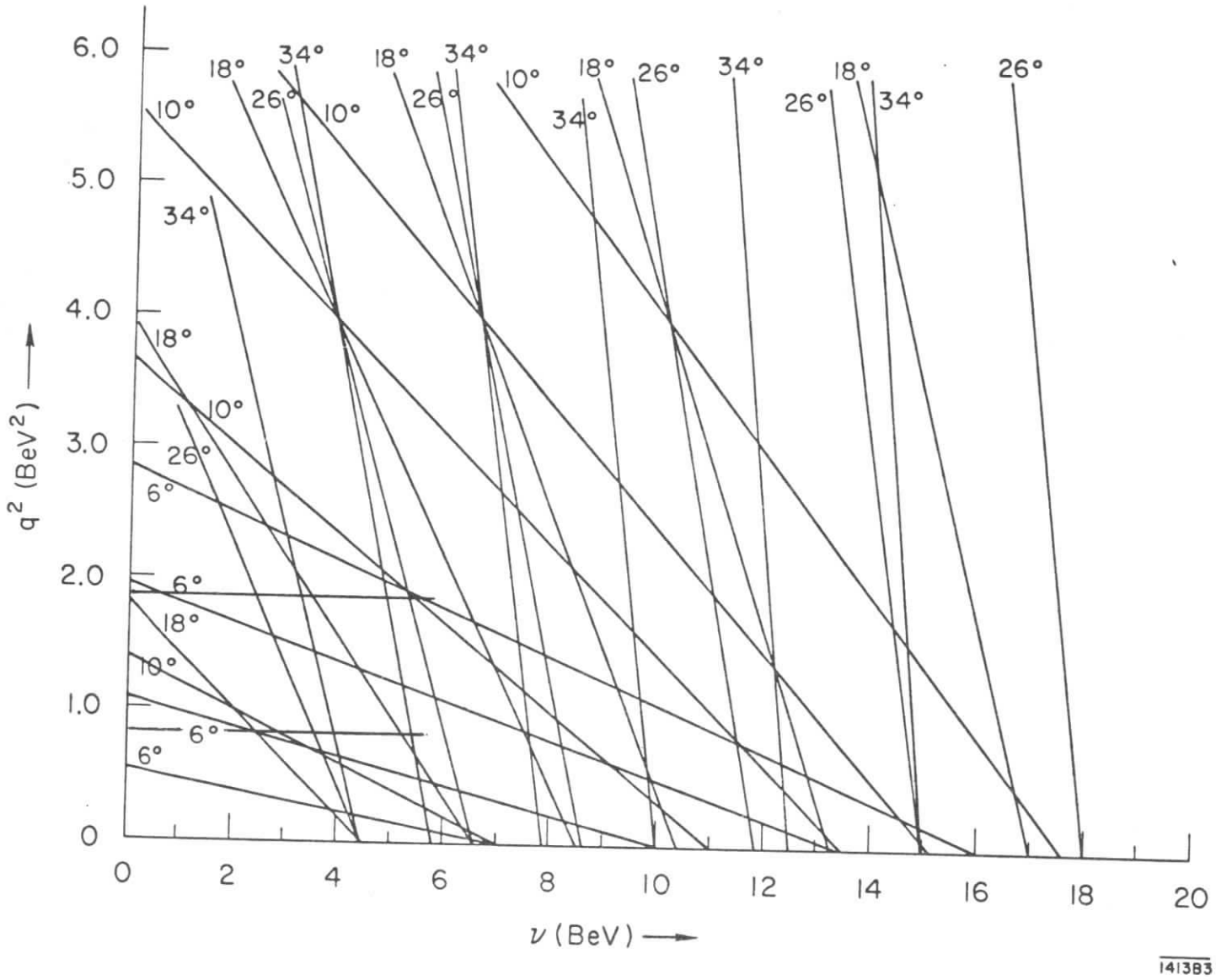
6.0
5.0
4.0
3.0
2.0
1.0
0
q^2 (BeV^2)
0
2
4
6
8
10
12
14
16
18
20
ν (BeV)
10°
18°
26°
34°
6°
141383

Fig. 2

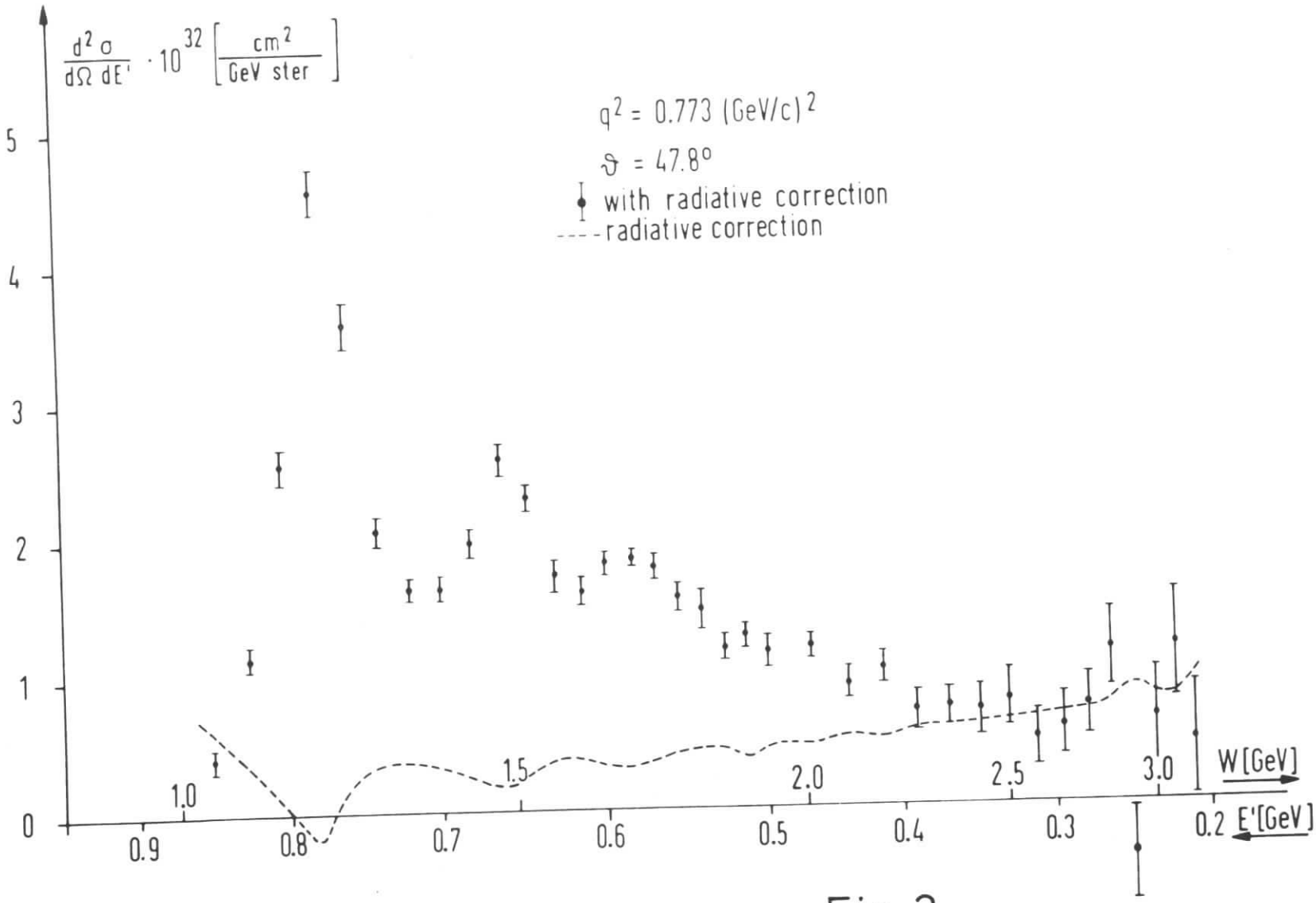
$\frac{d^2\sigma}{d\Omega\, dE'} \cdot 10^{32} \left[\frac{cm^2}{GeV\ ster}\right]$
$q^2 = 0.773\ (GeV/c)^2$
$\vartheta = 47.8°$
with radiative correction
radiative correction
5
4
3
2
1
0
1.0
0.9
0.8
0.7
0.6
1.5
0.5
0.4
2.0
0.3
2.5
3.0
0.2
W[GeV]
E'[GeV]

Fig. 3

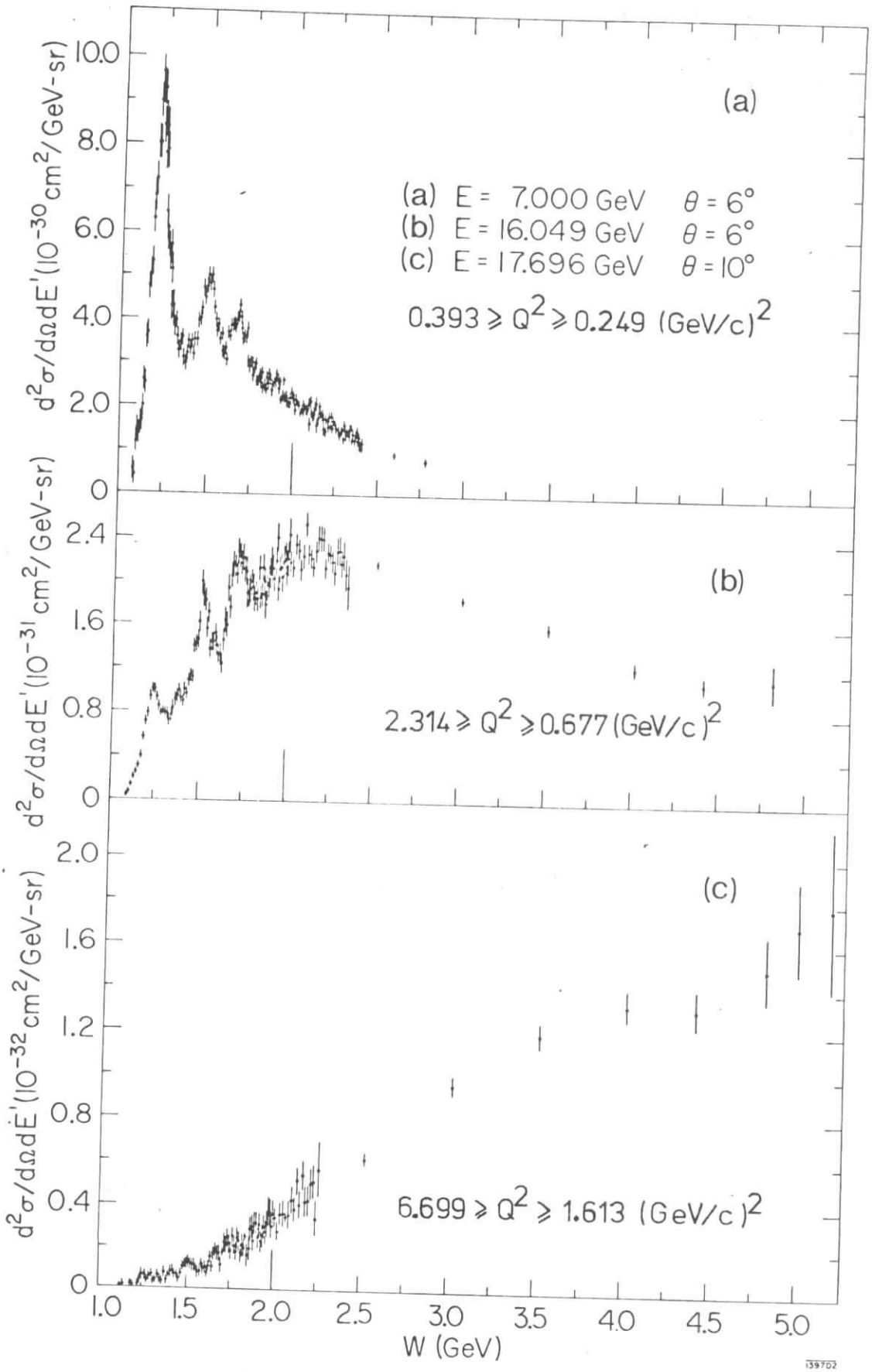
(a)
(a) E = 7.000 GeV θ = 6°
(b) E = 16.049 GeV θ = 6°
(c) E = 17.696 GeV θ = 10°
0.393 ≥ Q² ≥ 0.249 (GeV/c)²
(b)
2.314 ≥ Q² ≥ 0.677 (GeV/c)²
(c)
6.699 ≥ Q² ≥ 1.613 (GeV/c)²
d²σ/dΩdE' (10⁻³⁰ cm²/GeV-sr)
d²σ/dΩdE' (10⁻³¹ cm²/GeV-sr)
d²σ/dΩdE' (10⁻³² cm²/GeV-sr)
W (GeV)
13702

Fig. 4

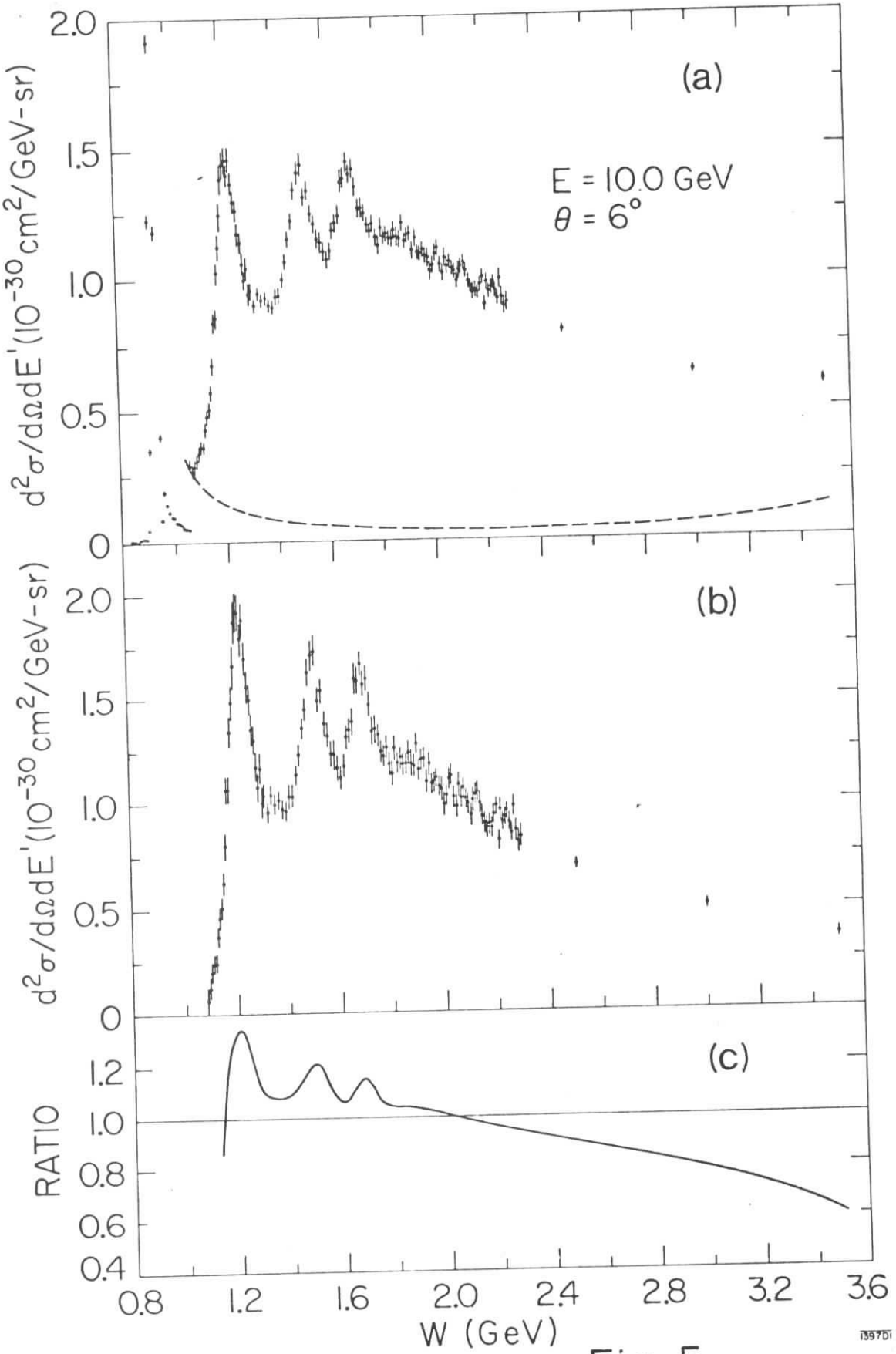
(a)
E = 10.0 GeV
θ = 6°
d²σ/dΩdE' (10⁻³⁰ cm²/GeV-sr)
(b)
d²σ/dΩdE' (10⁻³⁰ cm²/GeV-sr)
(c)
RATIO
W (GeV)
13970i

Fig. 5

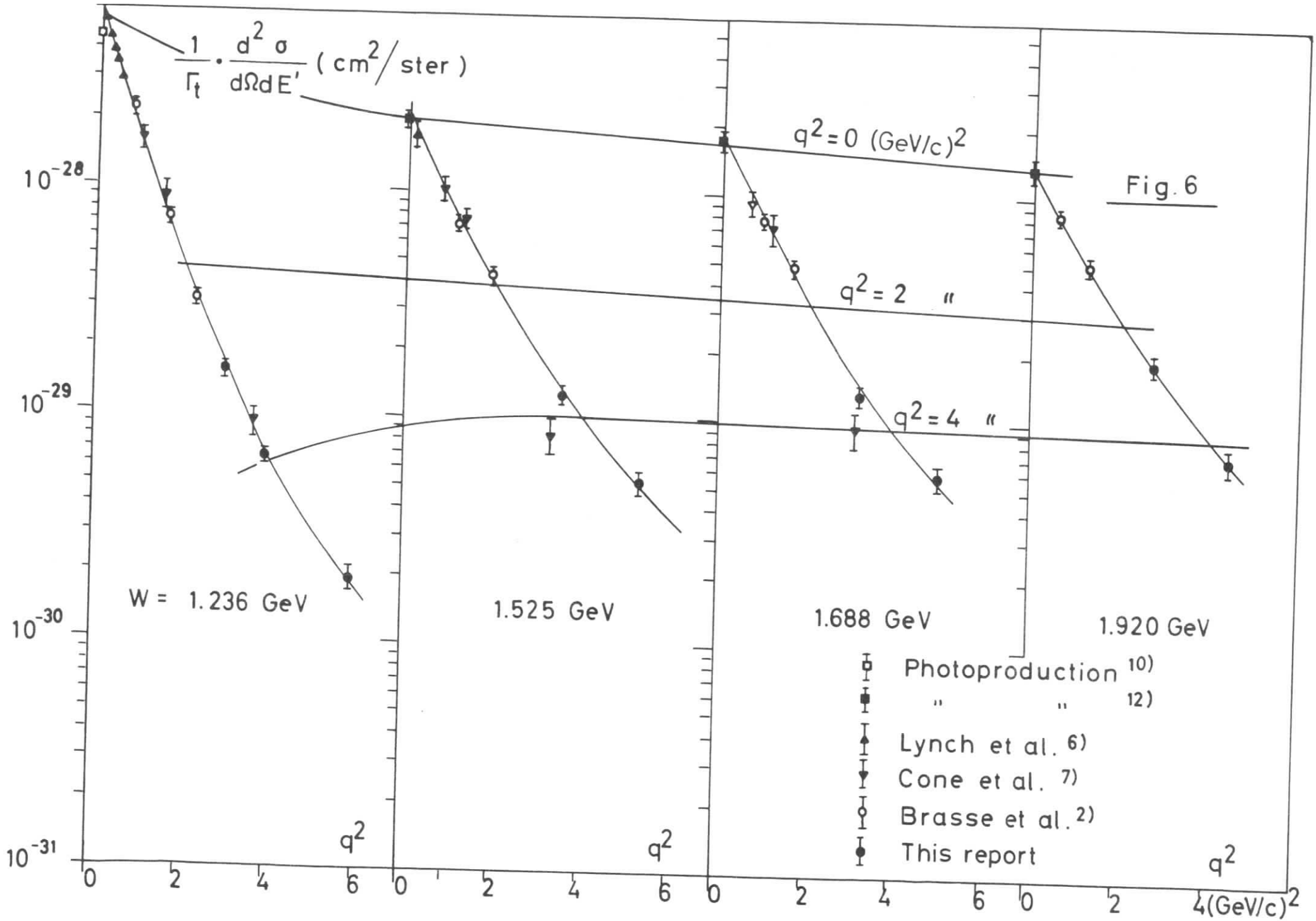
$\frac{1}{\Gamma_t} \cdot \frac{d^2\sigma}{d\Omega dE'}$ (cm^2/ster)
$q^2 = 0$ (GeV/c)^2
$q^2 = 2$ "
$q^2 = 4$ "
10^{-28}
10^{-29}
10^{-30}
10^{-31}
W = 1.236 GeV
1.525 GeV
1.688 GeV
1.920 GeV
q^2
0 2 4 6
4 (GeV/c)^2
Photoproduction 10)
" " 12)
Lynch et al. 6)
Cone et al. 7)
Brasse et al. 2)
This report

Fig. 6

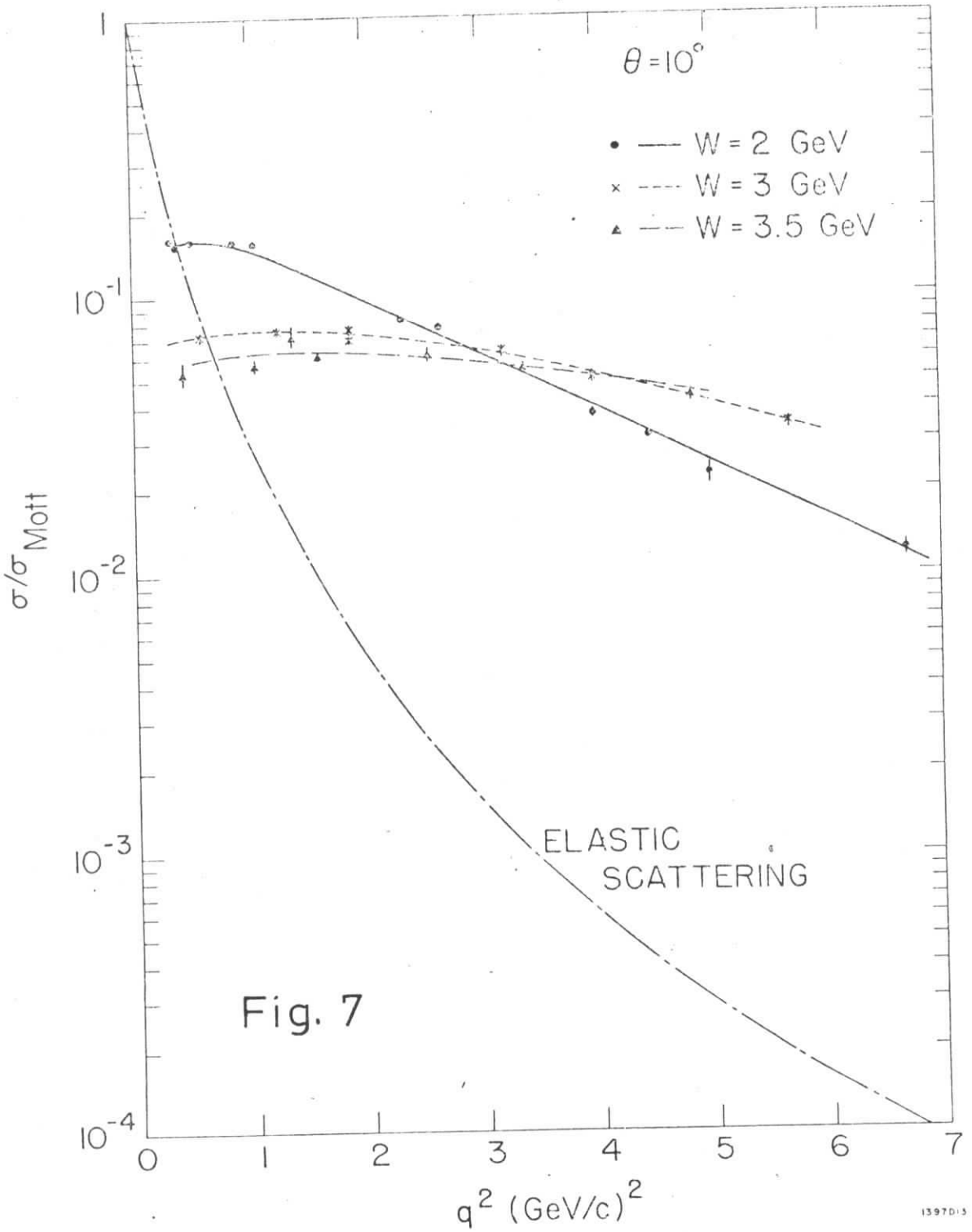
θ = 10°
W = 2 GeV
W = 3 GeV
W = 3.5 GeV
ELASTIC SCATTERING
σ/σ Mott
q² (GeV/c)²
1
10⁻¹
10⁻²
10⁻³
10⁻⁴
0
1
2
3
4
5
6
7
1397D13

Fig. 7

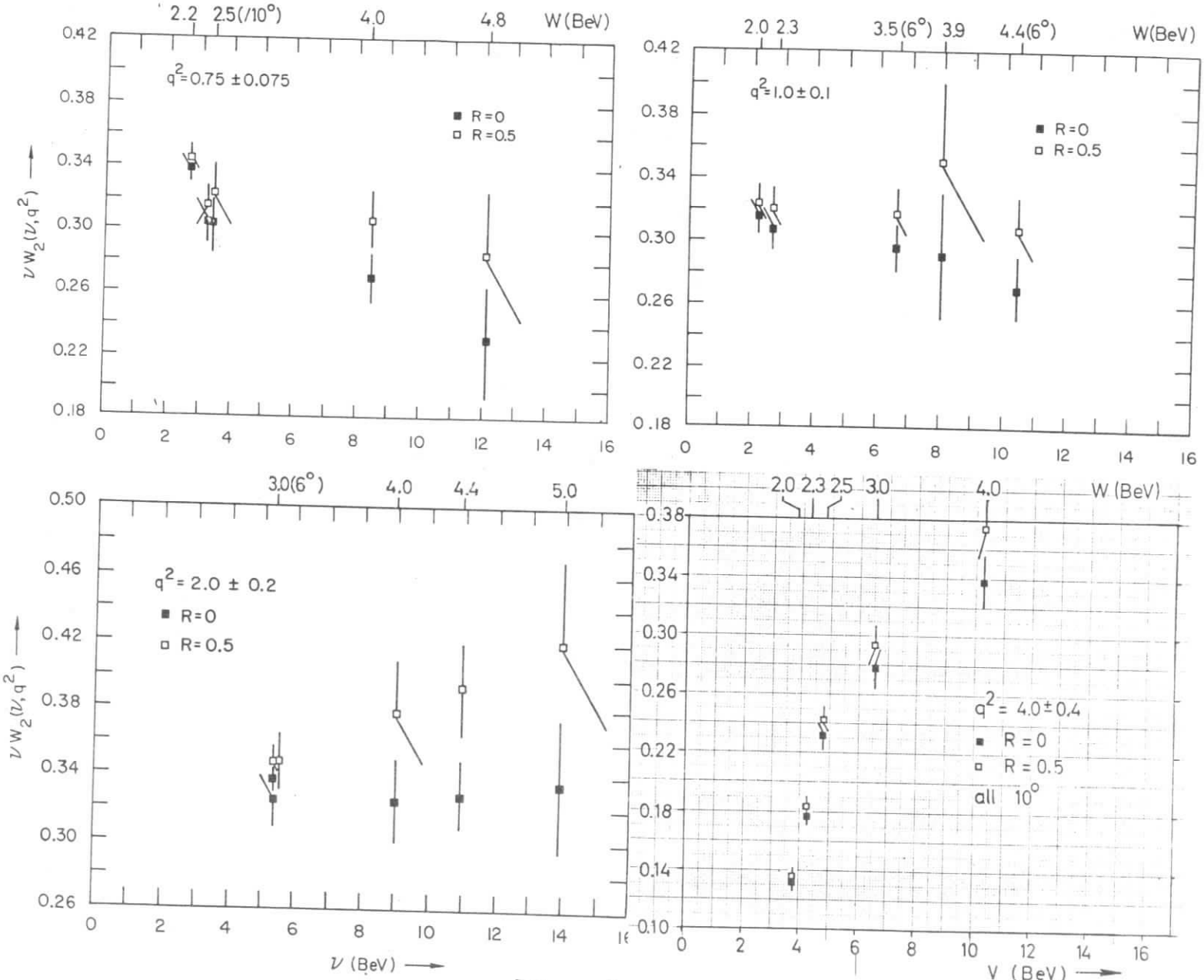
2.2 2.5(/10°) 4.0 4.8 W(BeV)
q^2=0.75 ±0.075
R=0
R=0.5
$\nu W_2(\nu, q^2)$
2.0 2.3 3.5(6°) 3.9 4.4(6°) W(BeV)
q^2=1.0±0.1
R=0
R=0.5
3.0(6°) 4.0 4.4 5.0
q^2= 2.0 ± 0.2
R=0
R=0.5
$\nu W_2(\nu, q^2)$
ν (BeV)
2.0 2.3 2.5 3.0 4.0 W (BeV)
q^2 = 4.0±0.4
R = 0
R = 0.5
all 10°
V (BeV)

Fig. 8

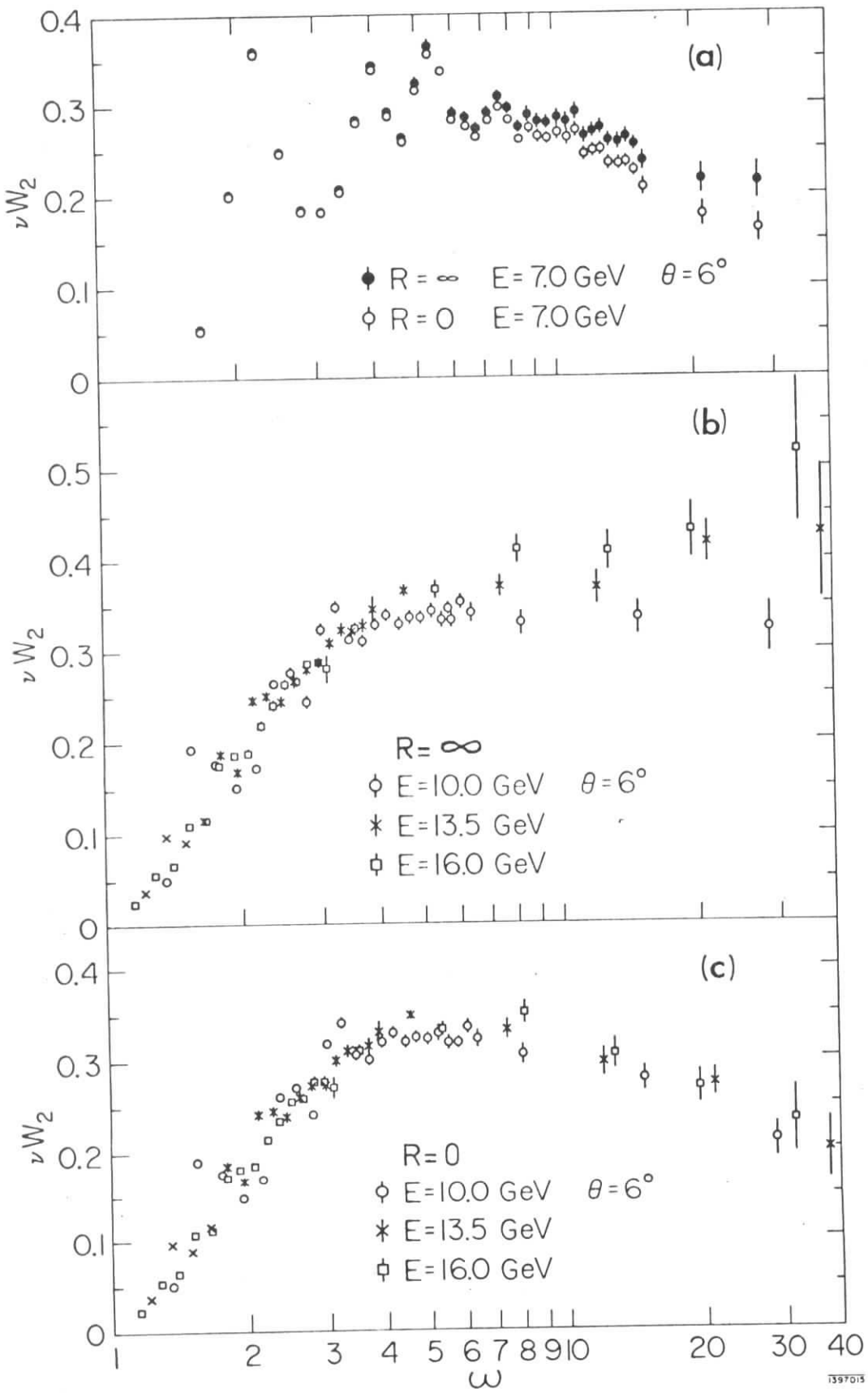
(a)
νW_2
R = ∞ E = 7.0 GeV θ = 6°
R = 0 E = 7.0 GeV
(b)
R = ∞
E = 10.0 GeV θ = 6°
E = 13.5 GeV
E = 16.0 GeV
(c)
R = 0
E = 10.0 GeV θ = 6°
E = 13.5 GeV
E = 16.0 GeV
ω
1 2 3 4 5 6 7 8 9 10 20 30 40
0 0.1 0.2 0.3 0.4 0.5
1397015

Fig. 9

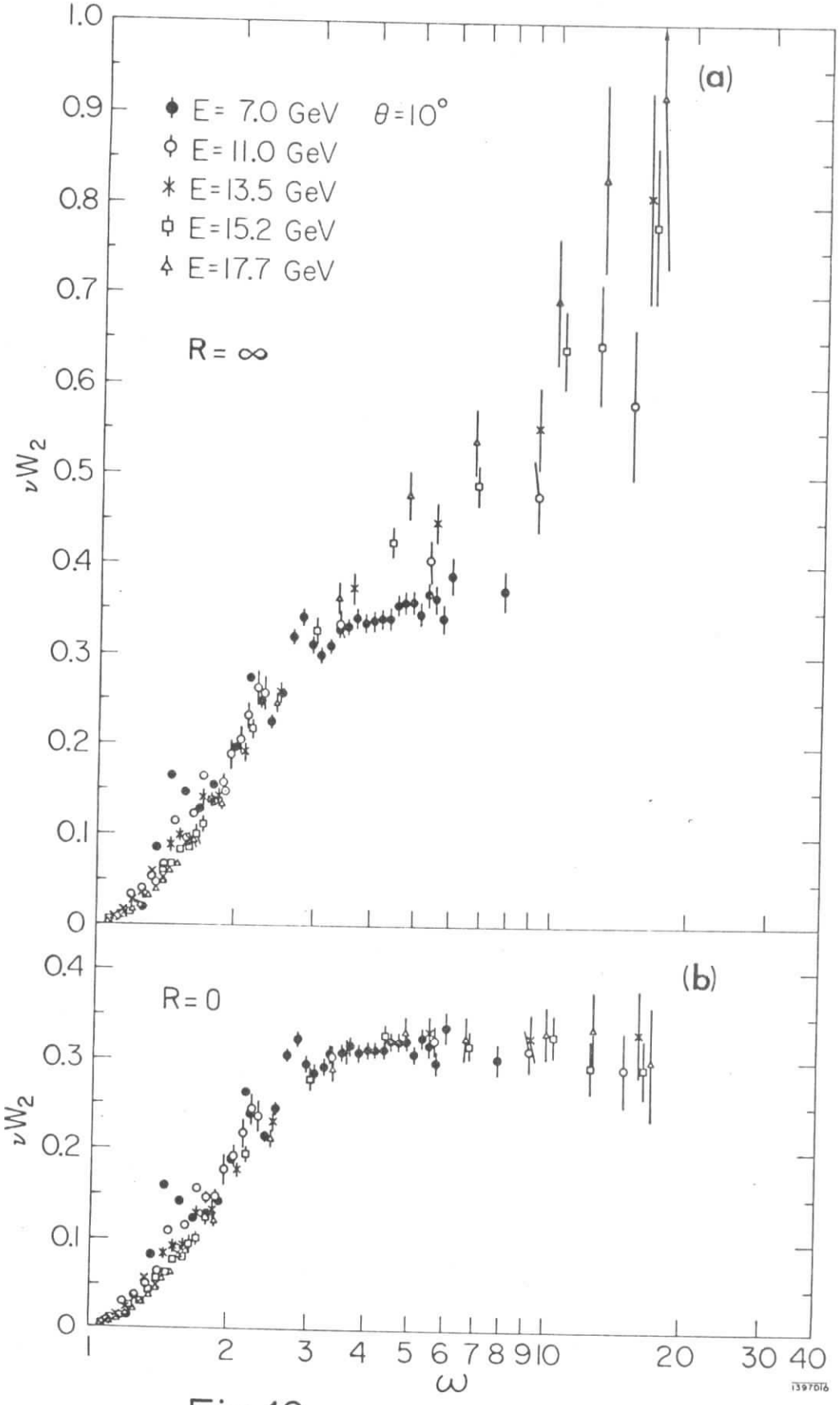
(a)
E = 7.0 GeV θ = 10°
E = 11.0 GeV
E = 13.5 GeV
E = 15.2 GeV
E = 17.7 GeV
R = ∞
νW2
(b)
R = 0
ω
1397016

Fig.10

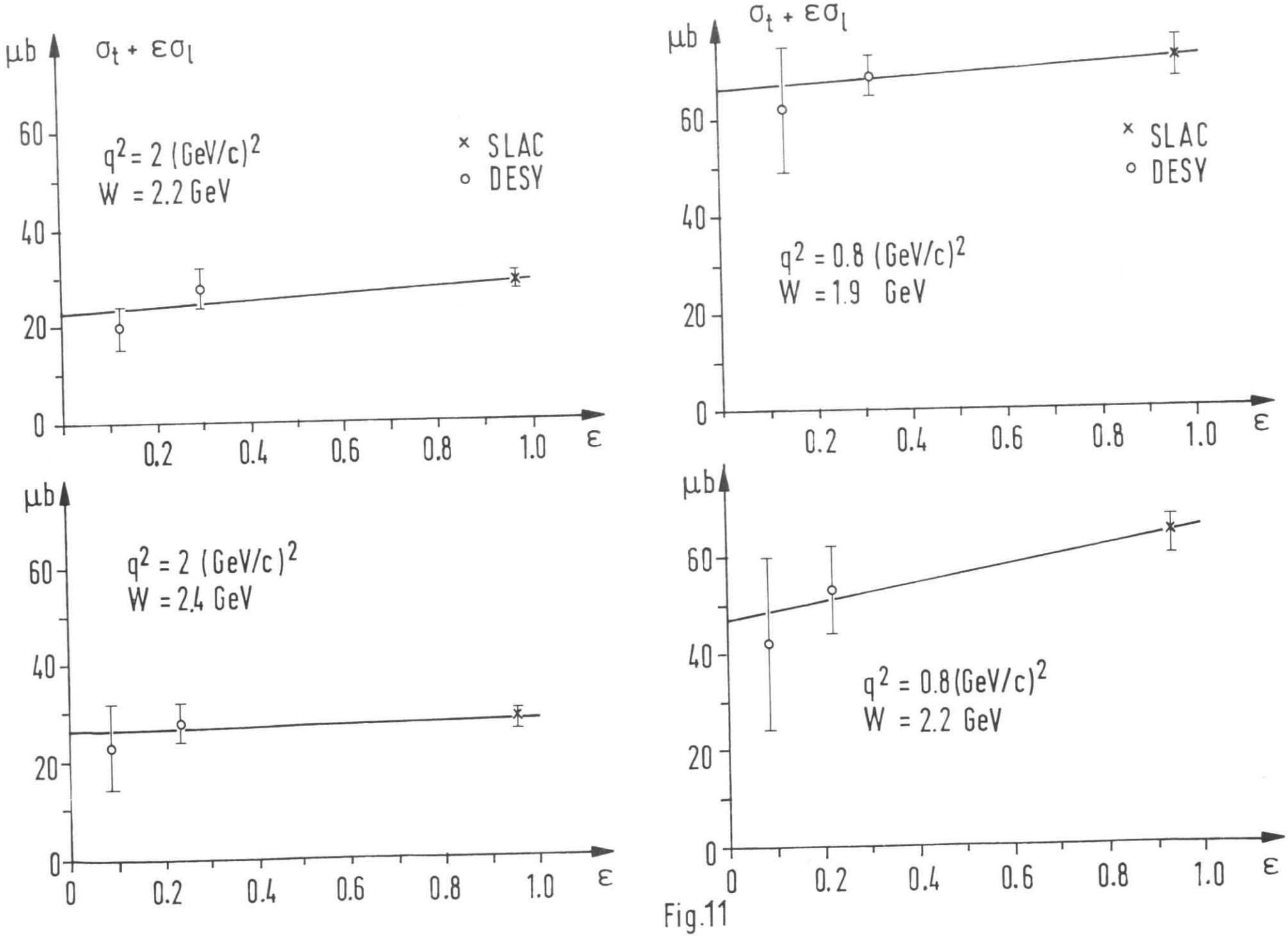
μb
$\sigma_t + \varepsilon\sigma_l$
$q^2 = 2$ (GeV/c)^2
W = 2.2 GeV
× SLAC
○ DESY
$q^2 = 0.8$ (GeV/c)^2
W = 1.9 GeV
W = 2.4 GeV
W = 2.2 GeV
0
20
40
60
0.2
0.4
0.6
0.8
1.0
ε

Fig.11

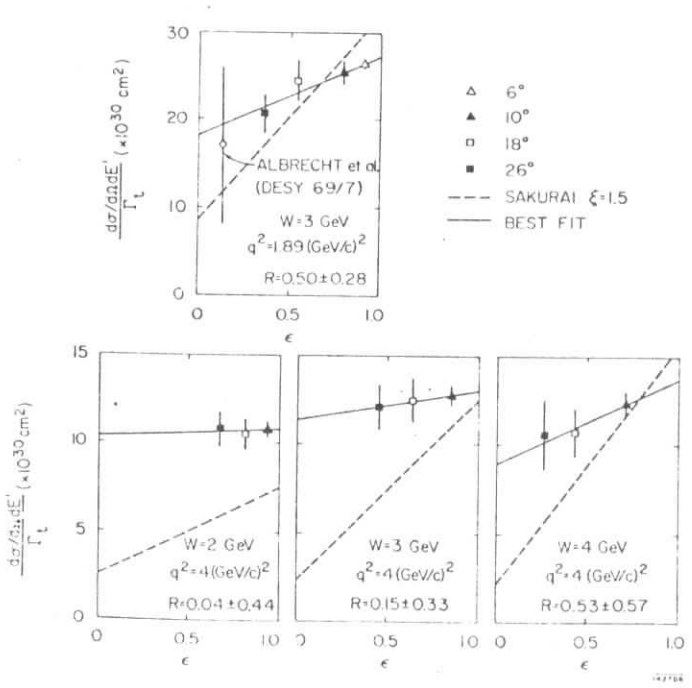
ALBRECHT et al.
(DESY 69/7)
W=3 GeV
q^2=1.89 (GeV/c)^2
R=0.50±0.28
6°
10°
18°
26°
SAKURAI ξ=1.5
BEST FIT
W=2 GeV
q^2=4 (GeV/c)^2
R=0.04±0.44
W=3 GeV
q^2=4 (GeV/c)^2
R=0.15±0.33
W=4 GeV
q^2=4 (GeV/c)^2
R=0.53±0.57
ε

Fig. 12

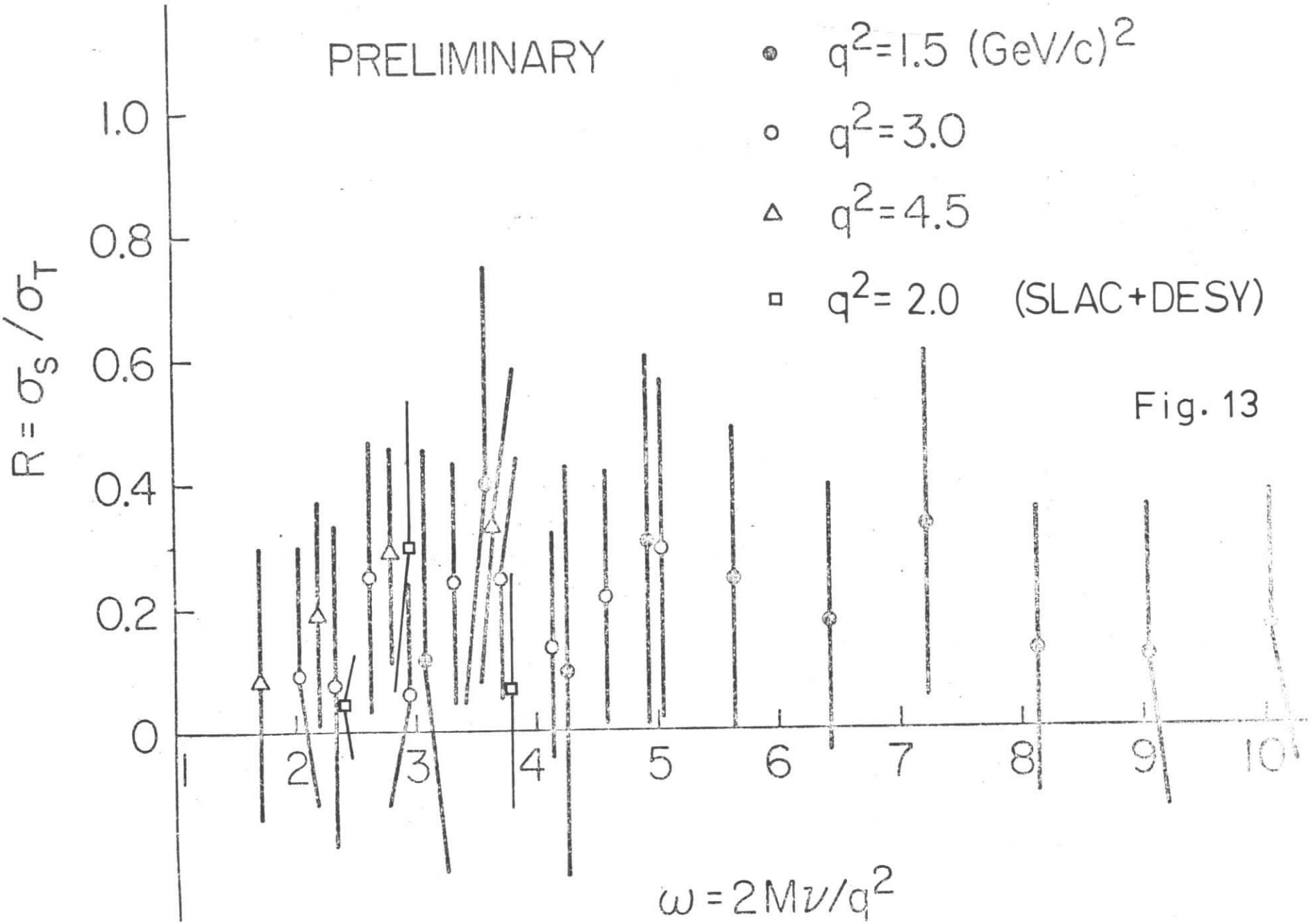
PRELIMINARY
q^2=1.5 (GeV/c)^2
q^2=3.0
q^2=4.5
q^2= 2.0 (SLAC+DESY)
$R = \sigma_S / \sigma_T$
1.0
0.8
0.6
0.4
0.2
0
1
2
3
4
5
6
7
8
9
10
$\omega = 2M\nu/q^2$

Fig. 13

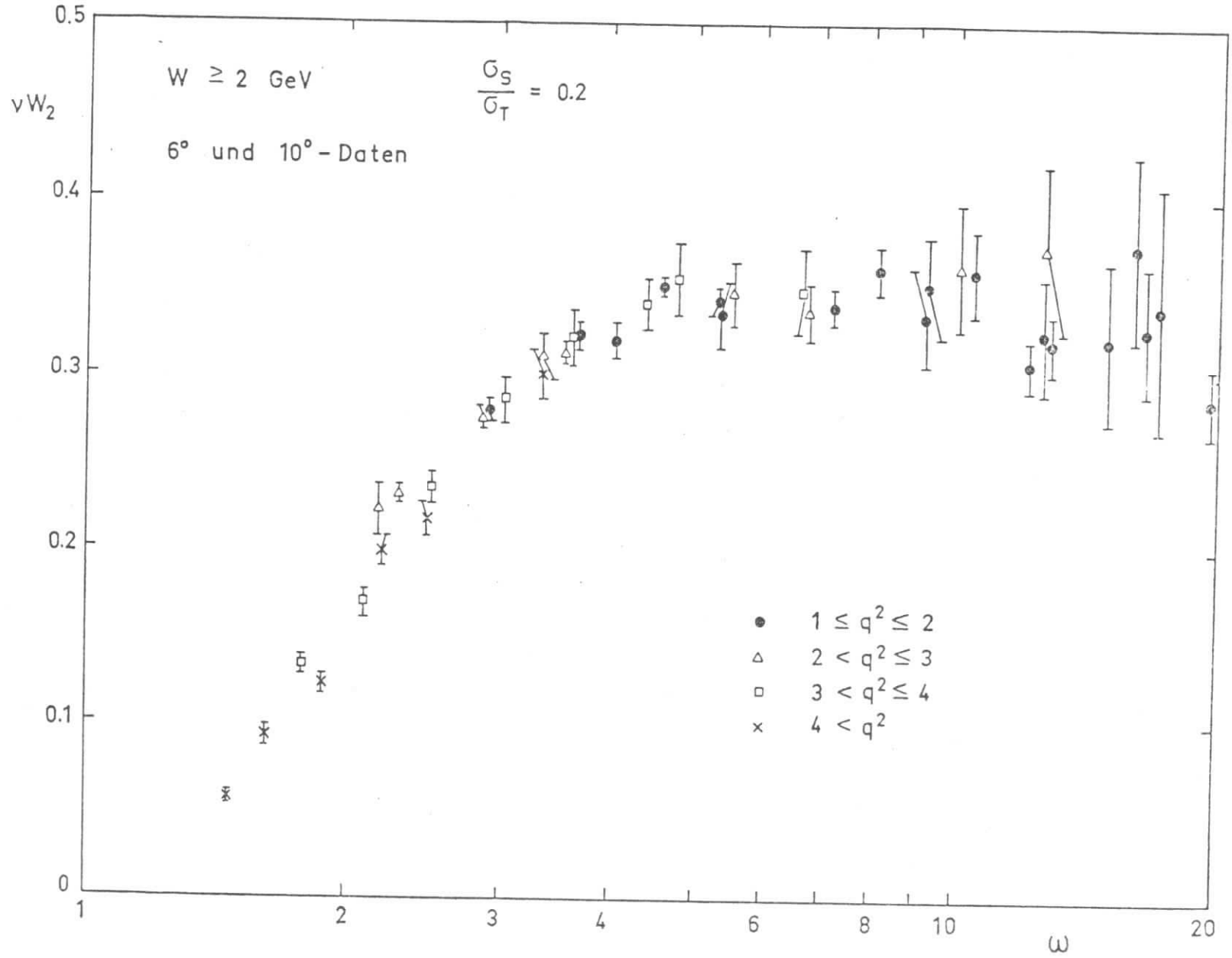
0.5
0.4
0.3
0.2
0.1
0
νW_2
W ≥ 2 GeV
$\frac{\sigma_S}{\sigma_T}$ = 0.2
6° und 10° - Daten
$1 \leq q^2 \leq 2$
$2 < q^2 \leq 3$
$3 < q^2 \leq 4$
$4 < q^2$
1
2
3
4
6
8
10
20
ω

Fig.14

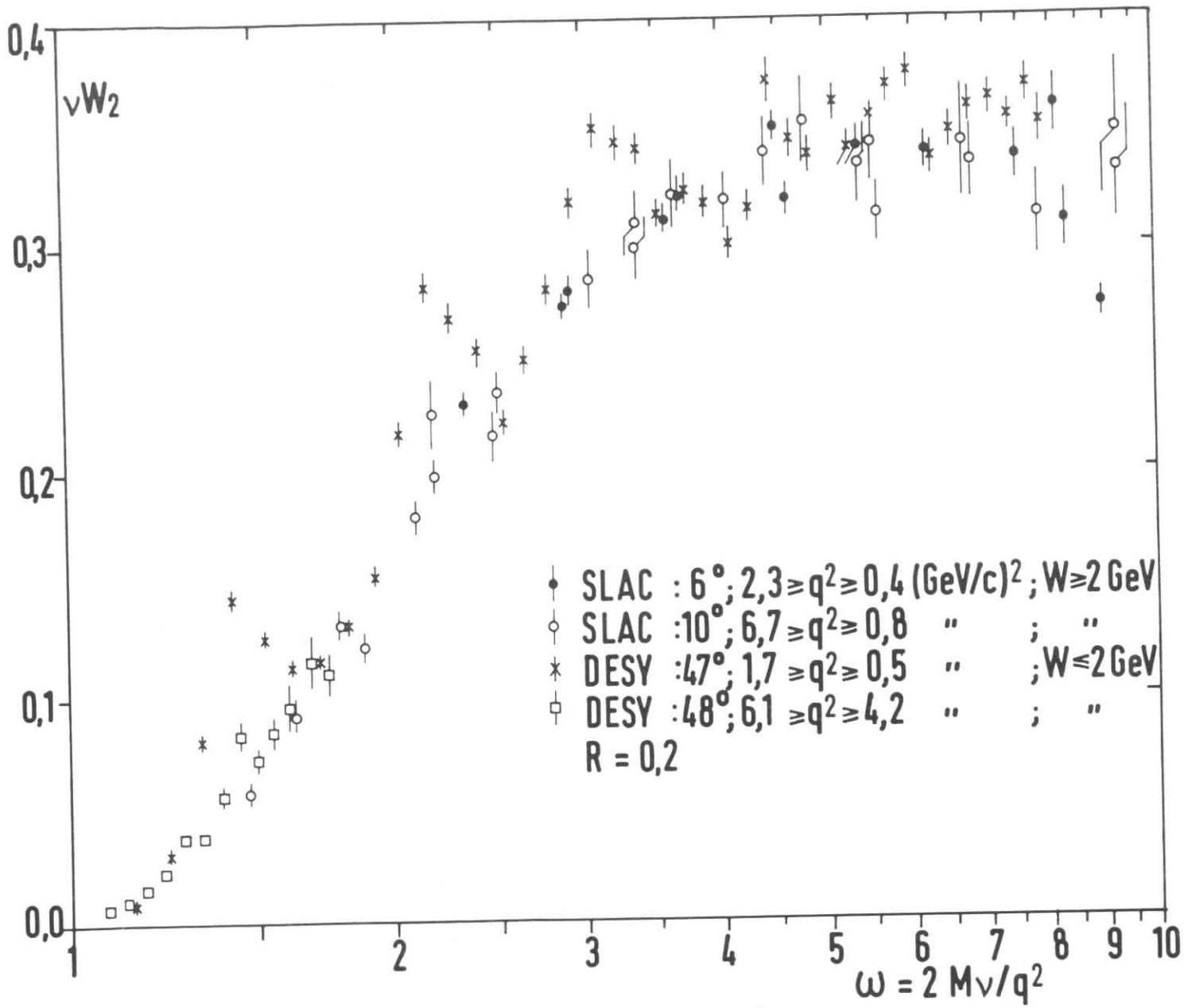
0,4
0,3
0,2
0,1
0,0
νW2
SLAC : 6°; 2,3 ≥ q² ≥ 0,4 (GeV/c)² ; W ≥ 2 GeV
SLAC :10°; 6,7 ≥ q² ≥ 0,8 " ; "
DESY :47°; 1,7 ≥ q² ≥ 0,5 " ; W ≤ 2 GeV
DESY :48°; 6,1 ≥ q² ≥ 4,2 " ; "
R = 0,2
1
2
3
4
5
6
7
8
9
10
ω = 2 Mν/q²

Fig.15

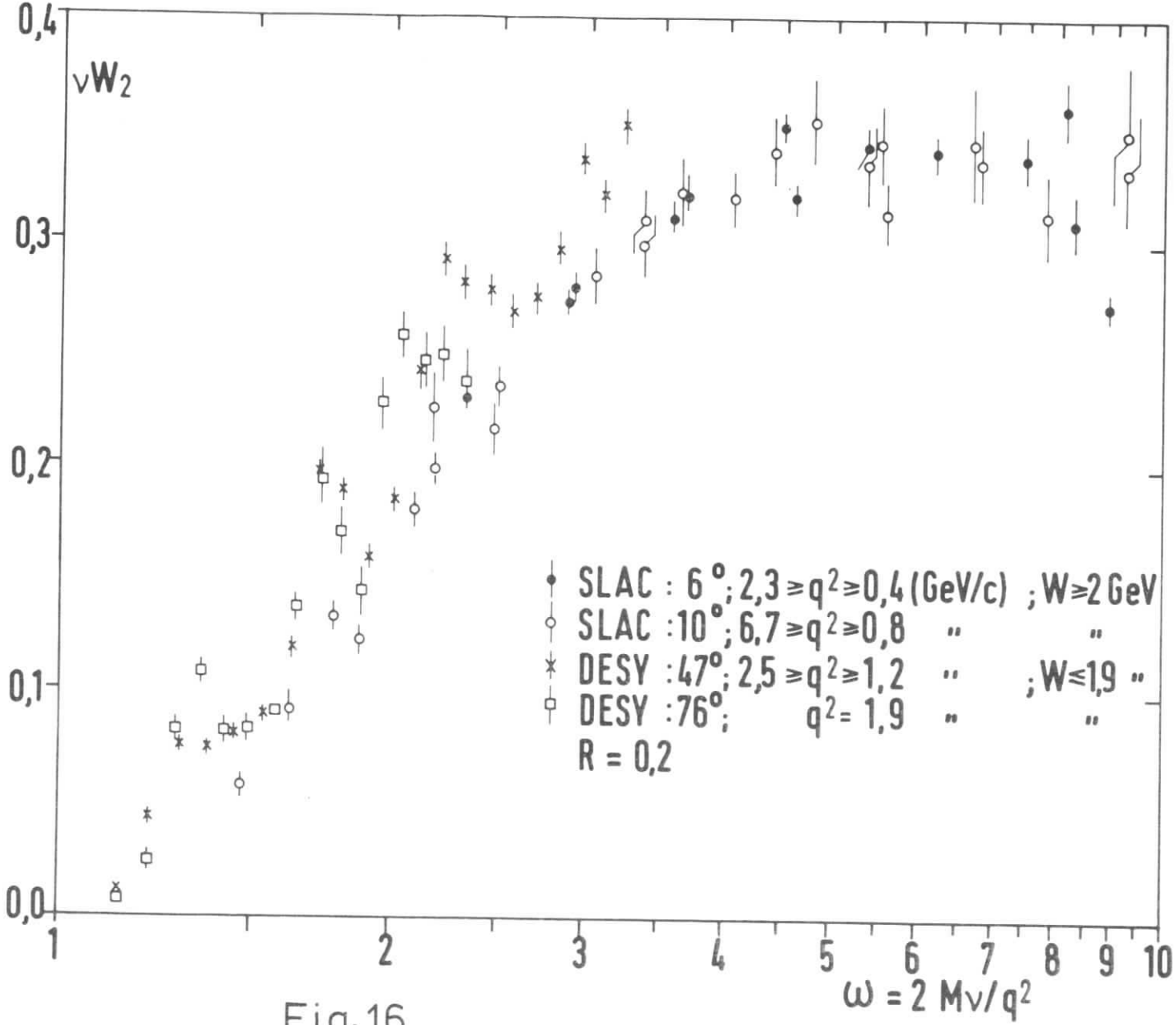
0,4
νW2
0,3
0,2
0,1
0,0
1
2
3
4
5
6
7
8
9
10
ω = 2 Mν/q²
SLAC : 6°; 2,3 ≥ q² ≥ 0,4 (GeV/c) ; W ≥ 2 GeV
SLAC : 10°; 6,7 ≥ q² ≥ 0,8 " "
DESY : 47°; 2,5 ≥ q² ≥ 1,2 " ; W ≤ 1,9 "
DESY : 76°; q² = 1,9 " "
R = 0,2

Fig. 16

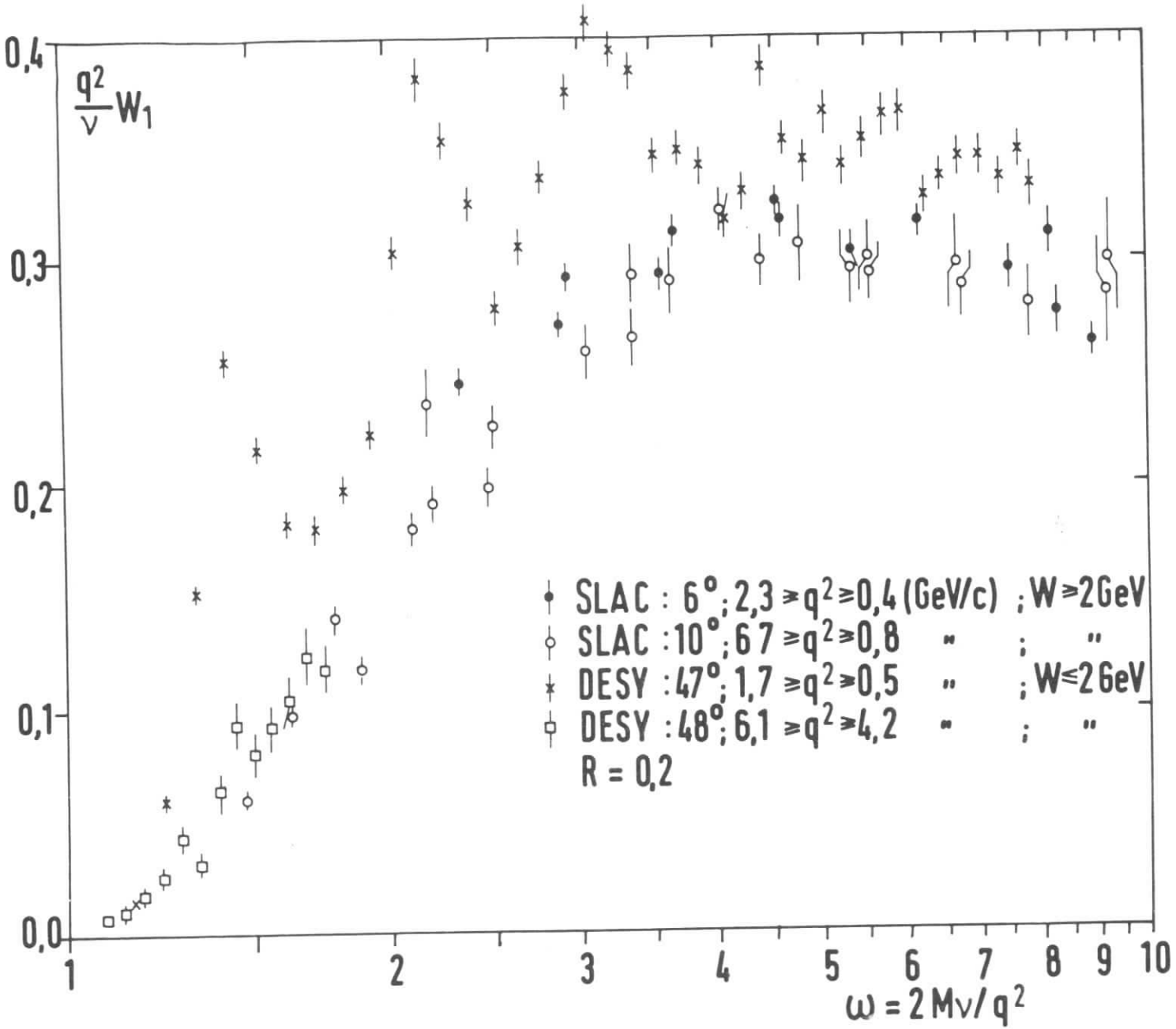
0,4
0,3
0,2
0,1
0,0
$\frac{q^2}{\nu} W_1$
SLAC : 6°; 2,3 ≥ q² ≥ 0,4 (GeV/c) ; W ≥ 2 GeV
SLAC : 10°; 6 7 ≥ q² ≥ 0,8 " ; "
DESY : 47°; 1,7 ≥ q² ≥ 0,5 " ; W ≤ 2 GeV
DESY : 48°; 6,1 ≥ q² ≥ 4,2 " ; "
R = 0,2
1
2
3
4
5
6
7
8
9
10
ω = 2 Mν / q²

Fig.17

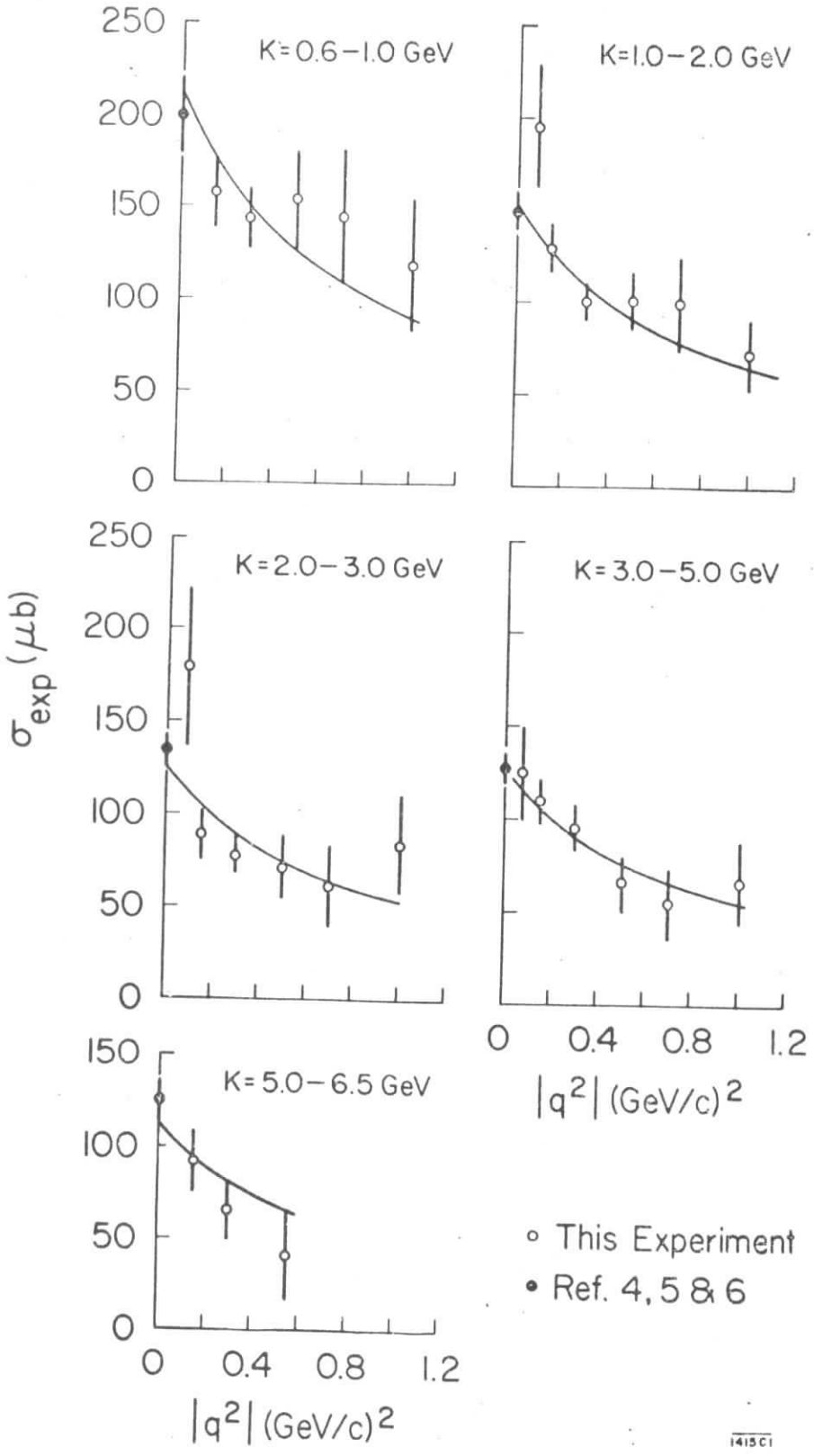
K=0.6–1.0 GeV
K=1.0–2.0 GeV
K=2.0–3.0 GeV
K=3.0–5.0 GeV
K=5.0–6.5 GeV
σ_{exp} (μb)
$|q^2|$ (GeV/c)^2
○ This Experiment
• Ref. 4, 5 & 6
1415C1

Fig. 18